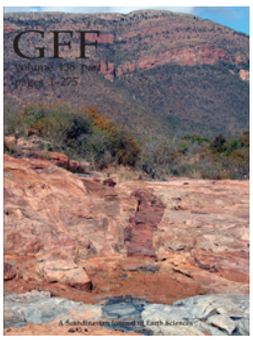

GFF

ISSN: 1103-5897 (Print) 2000-0863 (Online) Journal homepage: http://www.tandfonline.com/loi/sgff20

Mafic magmatism in the Bakhuis Granulite Belt (western Suriname): relationship with charnockite magmatism and UHT metamorphism

Martijn Klaver, Emond W.F. de Roever, Antonia C.D. Thijssen, Wouter Bleeker, Ulf Söderlund, Kevin Chamberlain, Richard Ernst, Jasper Berndt & Armin Zeh

To cite this article: Martijn Klaver, Emond W.F. de Roever, Antonia C.D. Thijssen, Wouter Bleeker, Ulf Söderlund, Kevin Chamberlain, Richard Ernst, Jasper Berndt & Armin Zeh (2016) Mafic magmatism in the Bakhuis Granulite Belt (western Suriname): relationship with charnockite magmatism and UHT metamorphism, GFF, 138:1, 203-218, DOI: 10.1080/11035897.2015.1061591

To link to this article: http://dx.doi.org/10.1080/11035897.2015.1061591

GFF, 2016
Vol. 138, No. 1, 203–218, http://dx.doi.org/10.1080/11035897.2015.1061591

Article

Mafic magmatism in the Bakhuis Granulite Belt (western Suriname): relationship with charnockite magmatism and UHT metamorphism

MARTIJN KLAVER[1], EMOND W.F. DE ROEVER[1], ANTONIA C.D. THIJSSEN[1], WOUTER BLEEKER[2], ULF SÖDERLUND[3,4], KEVIN CHAMBERLAIN[5], RICHARD ERNST[6], JASPER BERNDT[7] and ARMIN ZEH[8]

Klaver, M., de Roever, E., Thijssen, A., Bleeker, W., Söderlund, U., Chamberlain, K., Ernst, R., Berndt, J. & Zeh, A., 2015: Mafic magmatism in the Bakhuis Granulite Belt (western Suriname): relationship with charnockite magmatism and UHT metamorphism. *GFF*, Vol. 138, No. 1, 203–218. © Geologiska Föreningen. doi: http://dx.doi.org/10.1080/11035897.2015.1061591

Abstract: The Bakhuis Granulite Belt (BGB) is a metamorphic terrain within the Guiana Shield that experienced ultrahigh-temperature (UHT) metamorphism at 2.07–2.05 Ga. In the southwest of the BGB, the Kabalebo charnockites were emplaced at ca. 1.99 Ga and thus postdate UHT metamorphism by at least 60 Myr. Two generations of gabbroic intrusions have been recognized within the BGB, which could act as a heat source for the two UHT events. A younger generation of tholeiitic "Charlie" gabbros yields a baddeleyite U/Pb age of 1971 ± 15 Ma. The presence of a metamorphic overprint indicates that the hornblende-bearing "Moi–Moi" metagabbros predate the Charlie gabbros. Large zircons with complex zoning patterns are found in a Moi–Moi metagabbro sample. The main growth domains of these zircons give an age of 1984 ± 4 Ma, which is indistinguishable from the surrounding charnockites. Matching trace element and Hf isotope characteristics indicate that the complex zircons are derived from the charnockites. We argue that the emplacement of the metagabbros and charnockite magmatism were contemporaneous and that zircon grains from the charnockitic melt were mechanically transferred to the gabbroic bodies during magma mingling. The new ages for the gabbroic bodies in the BGB confirm that they are contemporaneous with, and the likely heat source for, charnockite magmatism, but that they are not associated with the 2.07–2.05 Ga UHT event. Furthermore, the new ages and recognition of the Moi–Moi metagabbros as an Alaskan-type complex provide the first direct evidence for late Transamazonian subduction zone magmatism in the Guiana Shield.

Keywords: geochronology; metagabbro; zircon geochemistry; Guiana Shield; Bakhuis Granulite Belt

[1]*Department of Geology and Geochemistry, VU University Amsterdam, De Boelelaan 1085, 1081HV Amsterdam, The Netherlands; martijn.klaver@vu.nl, ederoever@ziggo.nl, acd.thijssen@gmail.com*
[2]*Geological Survey of Canada, 601 Booth Street, Ottawa, Ontario, Canada, K1A 0E8; wbleeker@nrcan.gc.ca*
[3]*Department of Geology, Lund University, Sölvegatan 12, SE-223 62 Lund, Sweden; ulf.soderlund@geol.lu.se*
[4]*Department of Geosciences, Swedish Museum of Natural History, SE-114 18 Stockholm, Sweden*
[5]*Department of Geology and Geophysics, University of Wyoming, 1000 E. University Ave., Dept. 3006, Laramie, WY 82071, USA; kchamber@uwyo.edu*
[6]*Department of Earth Sciences, Carleton University, 1125 Colonel By Drive, Ottawa, Ontario, Canada, K1S 5B6; richard.ernst@ernstgeosciences.com*
[7]*Institute for Mineralogy, Westfälische Wilhelms-Universität Münster, Corrensstrasse 24, D-48149 Münster, Germany; jberndt@uni-muenster.de*
[8]*Institute for Geosciences, Goethe University Frankfurt; Altenhöferallee 1, D-60438 Frankfurt, Germany; a.zeh@uni-frankfurt.de*
Manuscript received 12 December 2014. Revised manuscript accepted 9 June 2015.

1. Introduction

1.1 Introduction

The Bakhuis Granulite Belt (BGB) in western Suriname is a striking feature within the Guiana Shield. The BGB comprises granulites that experienced ultrahigh-temperature (UHT) metamorphism (peak PT of 1000–1050°C at 0.85 GPa) at the end of the main phase of the Transamazonian Orogeny at 2073–2055 Ma (De Roever et al. 2003b; Klaver et al. 2015). The southwestern part of the BGB is dominated by a 30 by 30 km body of orthopyroxene-bearing granitoids, the Kabalebo

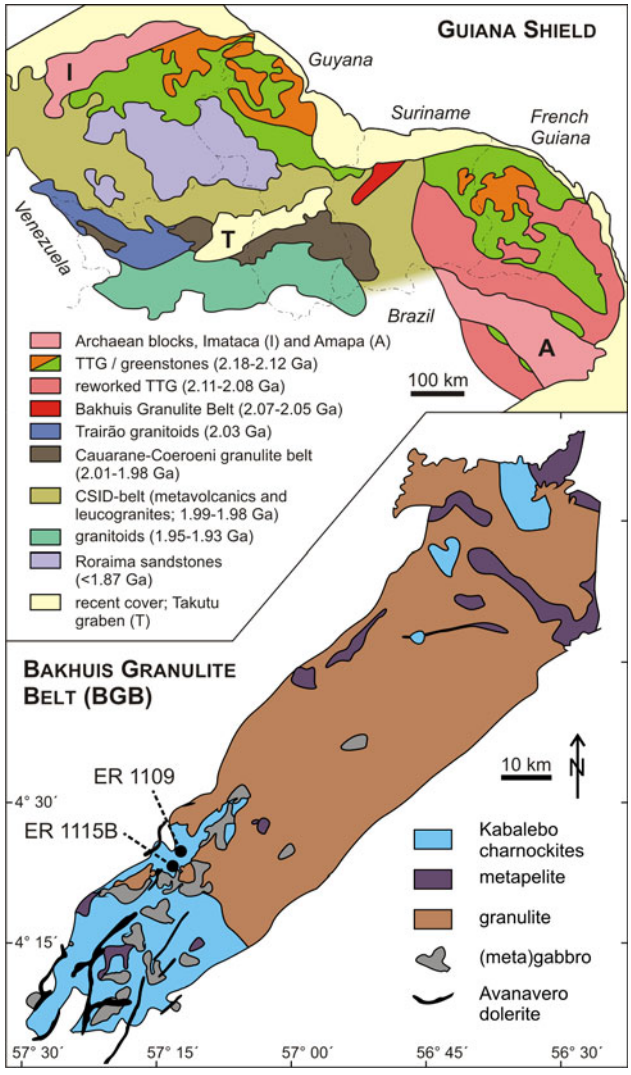

Fig. 1. Geological overview map of the Transamazonian Guiana Shield (top) and detailed map of the Bakhuis Granulite Belt (bottom, shown in red in the Guiana Shield map). The sampling locations of the two samples are indicated. Figure adapted from Klaver et al. (2015) and reproduced with permission from Elsevier.

charnockites (Fig. 1). The Kabalebo charnockites yield crystallization temperatures of 960–990°C and are the product of high-temperature, anhydrous melting of the granulite suite, but their emplacement at 1993–1984 Ma postdates UHT metamorphism by 60–90 Myr (Klaver et al. 2015). Hence, Klaver et al. (2015) concluded that the BGB experienced two separate events in which temperatures in excess of 950°C were reached in the lower crust: UHT metamorphism at 2.07–2.05 Ga followed by intrusion of the Kabalebo charnockites at 1.99 Ga. The origin of the two UHT events in the BGB is still poorly understood. A major unresolved issue regarding UHT metamorphism and anhydrous granitoid magmatism in general is the source of the heat required to achieve these conditions. It has been demonstrated that UHT conditions cannot be reached in normal collisional orogens without the need of high concentrations of heat-producing elements and crustal thickening (e.g. Collins 2002; Clark et al. 2011), neither of which is viable for the BGB (Klaver et al., 2015). Therefore, an external heat source such as contemporaneous mafic magmatism, either as underplating or as intrusions, is often evoked as a mechanism to explain the extreme heating (e.g. Westphal et al. 2003; Liu et al. 2006; Zhang et al. 2010; Guo et al. 2012; Peng et al. 2012; Santosh et al. 2012).

Gabbroic and metagabbroic intrusions are abundant in the BGB and are concentrated in the southwest together with the charnockites. On the basis of ambiguous field relationships, Klaver et al. (2015) proposed that the (meta)gabbros intruded contemporaneously with the charnockites at ca. 1.99 Ga and were therefore the likely heat source required for the high-temperature melting, but geochronological confirmation was lacking. In this model, the UHT metamorphic event at 2.07–2.05 Ga appears not to be coeval with mafic magmatism or significant crustal melting in the BGB or nearby Guiana Shield, but is related to mantle upwelling in a slab tear (Delor et al. 2003a; Klaver et al. 2015). A variable metamorphic overprint in the gabbros points towards the presence of more than one generation of gabbroic intrusions in the BGB. In the absence of absolute dating of these (meta)gabbroic intrusions, it remains unclear if there are indeed multiple generations and whether these are associated with the first or the second UHT event. In this paper, we present the first geochronological constraints for mafic magmatism in the BGB to validate the model proposed by Klaver et al. (2015). Two distinct mafic intrusive samples have been dated, a zircon-bearing metagabbro and a baddeleyite-bearing cumulate gabbronorite, with the aim to elucidate the complex history of the BGB in particular and UHT metamorphism in general.

In addition, this paper aims to explore the reliability of U/Pb ages obtained on zircon in gabbroic rocks. Mafic rocks are often undersaturated in Zr and generally do not crystallize zircon. Primary zircon can form in late-stage melt pockets that have become significantly enriched in Zr and silica. Alternatively, zircon in gabbroic rocks can be xenocrystic in origin, in which case zircon U/Pb dating will yield a maximum age. To distinguish between xenocrystic and primary zircon, detailed textural analysis can be helpful, but interpretation of zircon textures remains ambiguous (e.g. Corfu et al. 2003). Zircon trace element and in particular Hf isotope composition are expected to have the potential to unequivocally establish the origin of zircon in mafic rocks. To test this hypothesis and to assess the origin of zircon in the metagabbro sample, we present a comprehensive data-set of *in situ* zircon trace element and Hf isotope data.

1.2 Geological setting of the Guiana Shield

The Guiana Shield constitutes the northern part of the Amazonian Craton and extends from east Venezuela across Guyana, Suriname and French Guiana to northern Brazil (Fig. 1). The shield was formed during the Transamazonian Orogeny (2.26–1.95 Ga) with the exception of Archaean blocks in the west (Imataca) and east (Amapa). The Transamazonian Orogeny can be divided into two stages (Delor et al. 2003a). During the main Transamazonian phase, southward subduction of oceanic crust led to the development of the North Guiana tonalite-trondhjemite-granodiorite (TTG) and greenstone belt at 2.18–2.12 Ga (Norcross et al. 2000; Delor et al. 2003a; Hildebrand et al. 2014; Padoan et al. 2014). Suturing of the TTG-greenstone belt with the West African Craton and Amapa block between 2.11 and 2.08 Ga (Delor et al. 2003a; da Rosa-Costa et al. 2006, 2008) stabilized the eastern part of the Shield. Ultrahigh-temperature metamorphism of subcreted detritus from

the TTG-greenstone belt, the Bakhuis granulites, at 2.07–2.05 Ga in the BGB (De Roever et al. 2003b; Klaver et al. 2015) postdates the amalgamation by at least 10 Myr and marks the end of the main Transamazonian phase. Northeast to northward subduction during the late Transamazonian phase is proposed to have been the cause of amphibolite- to granulite-facies metamorphism in the Cauarane-Coeroeni Belt at 2.01–1.99 Ga (Fraga et al. 2009; Nadeau et al. 2013; De Roever et al. in press), charnockite magmatism in the BGB at 1.99 Ga (Klaver et al., 2015) and the development of a belt of felsic metavolcanic rocks and subvolcanic granites, the Cuchivero-Surumu-Iwokrama-Dalbana (CSID) belt, at 1.99–1.98 Ga (Reis et al. 2000; Delor et al. 2003a; Nadeau et al. 2013; De Roever et al. in press). The CSID-belt was subsequently intruded by biotite granite and S-type granites at 1.96–1.95 Ga (Fraga et al. 2009; De Roever et al. in press). The final stabilization of the Guiana Shield is constrained by the onset of deposition of the unfolded Roraima sandstones at 1.90–1.87 Ga (Santos et al. 2003; Minter 2006). The southwest part of the Guiana Shield is dominated by post-collisional, <1.90 Ga granitoid magmatism (Santos et al. 2004; Kroonenberg & de Roever 2010).

1.3 *Late Transamazonian mafic intrusions*

Reconnaissance work by the Geological and Mining Service of Suriname in the 1960's and 1970's led to the identification of 100 or more mafic to ultramafic intrusions of 0.5–20 km in size in western and central Suriname. Most of these bodies share a number of characteristics (Bosma et al. 1983): (i) associated gabbroic and ultramafic rocks within one body; (ii) a rough vertical zoning within a single body from peridotite or pyroxenite in the lower part to gabbronorite in the upper regions, but without obvious modal layering in individual outcrops or drill cores; (iii) coarse, cm-sized hornblende, often occurring as a poikilitic or intercumulus phase and (iv) orthopyroxene as a common constituent. On the basis of these common characteristics, the mafic to ultramafic bodies were loosely grouped as the De Goeje-type gabbros on the 1977 geological map of Suriname. This name, however, should be abandoned as it comprises more than one generation of mafic intrusions. For instance, the Pt-bearing body at the type locality in the De Goeje Mountains is associated with the North Guiana TTG-greenstone belt and can be correlated with similar bodies in French Guiana with an age of 2.15 Ga (Delor et al., 2003b). Mafic to ultramafic intrusions in the BGB, Coeroeni gneisses and felsic metavolcanic rocks in western Suriname are considerably younger. Their occurrence as xenoliths in the 1949 ± 12 Ma biotite granite (zircon Pb–Pb evaporation; De Roever et al. in press) and intrusive contacts in the 1.99–1.98 Ga CSID-belt indicate that these bodies are part of the late Transamazonian phase (2.01–1.95 Ga). Gabbroic bodies that intruded the Coeroeni gneisses and BGB display a medium to high-grade metamorphic overprint, such as granoblastic recrystallization, but without the development of penetrative or marked marginal foliation. This suggests that these bodies postdate the kinematic metamorphism in the gneiss belts. Comparable bodies have been described in the Cauarane-Coeroeni Belt and CSID-belt in southern Guyana (Berrangé 1977) and Roraima State in northern Brazil (Gibbs & Barron 1993). Due to their regional distribution, these late Transamazonian mafic to ultramafic bodies may be considered as a yet undated large igneous province (LIP; e.g. Ernst 2014) in the south-central Guiana Shield. The late Transamazonian gabbroic intrusions are clearly distinct from and crosscut by younger mafic dyke swarms in the central part of the Guiana Shield. These include the 1795–1793 Ma Avanavero dolerite dykes and sills (Reis et al. 2013), which lack a metamorphic overprint and are characterized by the common presence of pigeonite, and the alkaline 1505 ± 5 Ma Käyser olivine dolerites (De Roever et al. 2003a).

Fieldwork during the last years has revealed that the late Transamazonian gabbro suite in the BGB consists of at least two generations of mafic intrusions. The first group comprises the Moi–Moi metagabbros (named after the type locality at the Moi–Moi waterfall; Fig. 2(a)), which most closely resemble the classical De Goeje-type gabbros. These mafic bodies show a variable degree of granoblastic recrystallization, but without development of a foliation, and are concentrated in the southwest of the BGB together with the Kabalebo charnockites (Fig. 1). The main distinguishing feature of the Moi–Moi metagabbros is the presence of coarse poikilitic, intercumulus amphibole. This primary, brown to olive-green hornblende is distinct from blue-green amphibole associated with the non-kinematic metamorphic overprint. A second generation of mafic intrusive bodies was recognized during recent fieldwork in the BGB. These Charlie gabbros to leucogabbros (named after the type locality downstream of Charlie Falls) are clearly distinguished from the Moi–Moi metagabbros by the lack of the medium- to high-grade metamorphic overprint and absence of the poikilitic hornblende. These tholeiitic gabbros contain lath-shaped plagioclase crystals up to 10 cm in length and pigeonite is a common phase (Fig. 2). On first sight, the Charlie gabbros might resemble the much younger Avanavero dolerite dykes and sills. The former, however, are characterized by complex corona textures around olivine that are absent in the Avanavero dolerites. So far, the Charlie gabbros have only been recognized within the BGB.

An anorthosite body of ca. 4 km in diameter in the centre of the BGB was dated by zircon Pb evaporation at 1980 ± 5 Ma (De Roever et al., 2003b). A xenocrystic origin for these zircons is unlikely as the anorthosite body is surrounded by granulites that yield 2073–2055 Ma ages corresponding to the UHT metamorphism or even older inherited ages and hence this zircon age appears to be reliable. The anorthosites are largely covered by high-grade bauxite, and two other bauxite occurrences in the BGB might cap similar anorthosite bodies.

2. Analytical methods

Baddeleyite was extracted at Lund University using the water-based Wilfley table technique of Söderlund & Johansson (2002). Due to very low concentration and <20 μm size of baddeleyite in sample ER 1115B, only two fractions of six and four grains, respectively, could be prepared for isotope dilution-thermal ionization mass spectrometer (ID-TIMS) U–Pb analysis. The selected baddeleyite grains were washed in alternating steps using nitric acid and water, and subsequently dissolved in a 10:1 $HF–HNO_3$ solution together with a mixed $^{236}U–^{233}U–^{205}Pb$ spike at 210°C overnight. The samples were loaded on a Re filament with 2 μl silica gel and analysed on a Thermo Finnigan TRITON TIMS at the Museum of Natural History in Stockholm. All peak intensities were measured on a secondary electron multiplier by peak switching. Data for Pb and U were collected in the temperature ranges 1230–1270°C and 1380–1420°C,

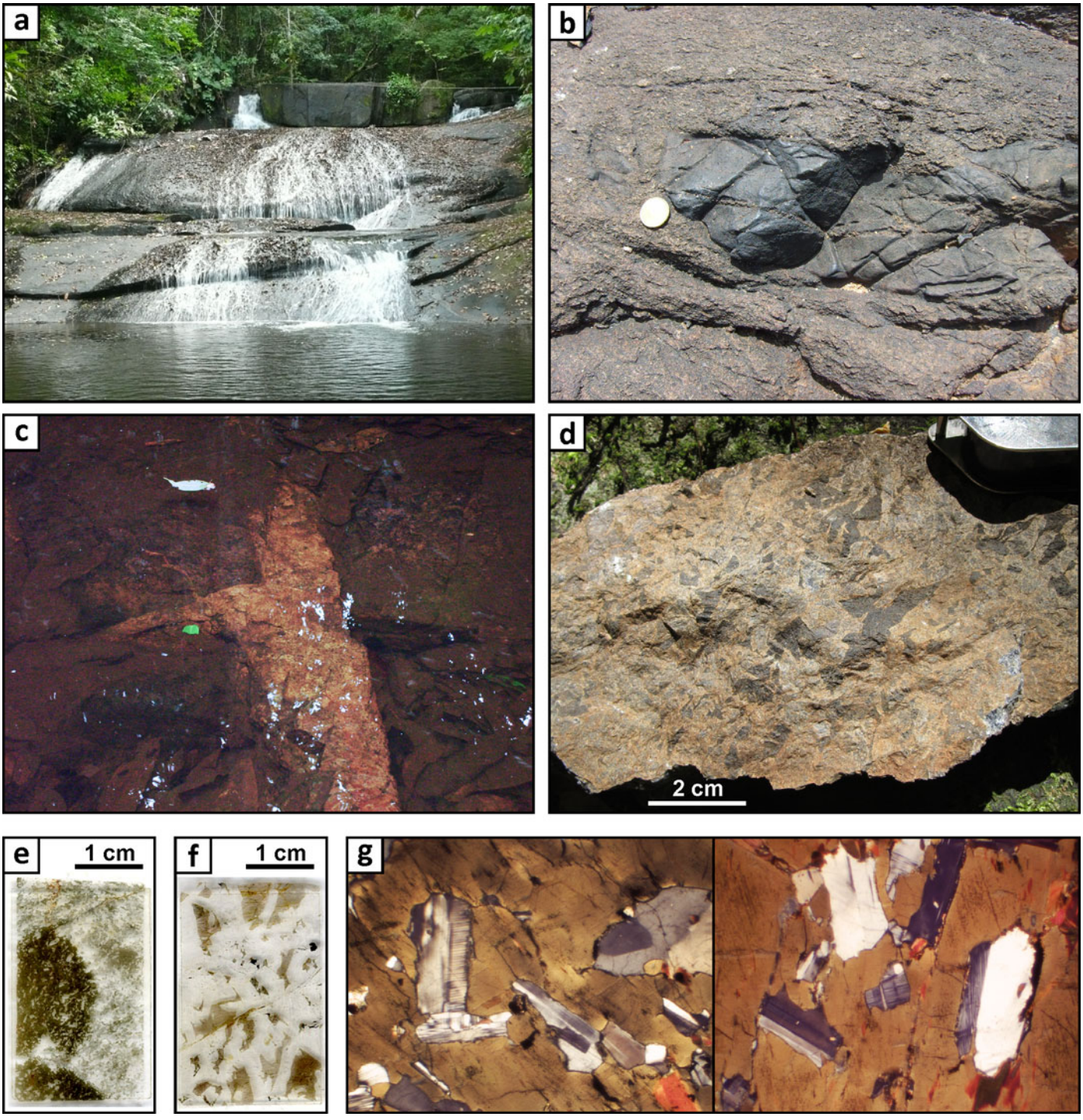

Fig. 2. Field relationships and petrography of the Charlie gabbros and Moi–Moi metagabbros. Due to the dense tropical rain forest, exposure is minimal and contacts between different lithologies are rarely visible. (a) The Moi–Moi waterfall, type locality of the metagabbro. The waterfall consists of Kabalebo charnockite; nearly continuous exposure of metagabbro starts 10 m behind the upper part of the waterfall and continues upstream for at least 1 km. The contact itself is not exposed. (b) Co-magmatic metadolerite enclave in the Kabalebo charnockites at the Krong Soela rapid. These metadolerite xenoliths are petrographically and geochemically identical to the larger metagabbro bodies. (c) Tapered charnockite vein intruding the Moi–Moi metagabbro near the contact at the Moi–Moi waterfall. (d) Charlie gabbro with network of euhedral, coarse plagioclase (light coloured minerals) with intercumulus pyroxene (grey). (e) Thin section scan of a Moi–Moi metagabbro sample showing two large poikilitic hornblende crystals enclosing euhedral plagioclase laths. (f) Thin section scan of a Charlie gabbro sample showing a typical dry crystallization sequence of coarse lath-shaped plagioclase before intercumulus pyroxene. (g) Photomicrographs (in XPL) of the Moi–Moi metagabbro sample from (e) illustrating the relict ophitic texture with large, poikilitic hornblende.

respectively. Isotope ratios were corrected for mass fractionation (0.1% per atomic mass unit for Pb), spike contribution, blank (1 pg Pb, 0.1 pg U) and initial common lead. Common Pb was corrected with isotope compositions from the model of Stacey & Kramers (1975) at the age of the sample.

Individual zircon domains in a polished thin section of metagabbro sample ER 1109 were dated by secondary-ion mass spectrometry (SIMS) using the CAMECA *ims*1270 ion microprobe at the University of California Los Angeles following methods described in Grove et al. (2003) and Schmitt et al. (2010). An 18 by 27 μm spot size was used for most pits, but an aperture in the transfer section of the secondary beam column reduced the effective sampling diameter to approximately 8 μm where analysis of narrow domains was required. The sample chamber was flooded with oxygen to enhance Pb secondary ion yields. The relative sensitivity of uranium and lead was calibrated by UO/U following the calibration method described by Compston et al. (1984) using the AS3 zircon standard (Paces & Miller, 1993; Schmitz et al., 2003). The results were corrected for initial common lead using the Stacey & Kramers (1975) model at the age of the sample. Age calculations were performed using Isoplot/Ex v. 4.15 (Ludwig, 2012) with decay constants from Steiger & Jäger (1977). Uncertainties are consistently reported at the 95% confidence level in the figures and text.

Additional zircon from sample ER 1109 was separated for trace element and Hf isotope analysis by laser-ablation inductively coupled plasma mass spectrometry (LA-ICPMS) using conventional heavy liquid and magnetic separation techniques. Zircon grains were handpicked from highly pure zircon fractions using a binocular microscope, set in epoxy resin and polished to reveal their interiors. The selected grains were imaged in transmitted light and by backscattered electron (BSE) and cathode-luminescence (CL). *In situ* Hf isotope analysis was performed at Goethe University Frankfurt by LA-MC-ICPMS following the methods outlined in Gerdes & Zeh, (2006, 2009). The laser was operated using a spot size of 50 μm, repetition rate of 5.5 Hz and an energy density of ca. 12 J/cm^2 during 40 s of data acquisition. Data were processed offline and corrected for isobaric interference and mass bias to $^{179}Hf/^{177}Hf = 0.7325$ to yield $^{176}Lu/^{177}Hf$ and $^{176}Hf/^{177}Hf$ ratios. Zircon reference material GJ-1 was used as an internal standard and results were normalized to a $^{176}Hf/^{177}Hf$ of 0.282000 for GJ-1 (Morel et al. 2008). Accuracy and reproducibility were verified by the repeated analysis of zircon reference materials GJ-1, Z91500, Plešovice and Temora-2, which yielded a $^{176}Hf/^{177}Hf$ of 0.282000 ± 0.000029 (2 SD, $n = 13$), 0.282280 ± 0.000040 ($n = 7$), 0.282455 ± 0.000024 ($n = 7$) and 0.282666 ± 0.000027 ($n = 2$), respectively. The results are available in the online Supplementary material.

Zircon trace element analysis by LA-ICPMS was performed at Westfälische Wilhelms-Universität Münster using a 193 nm excimer laser (Analyte G2, Photon Machines) connected to a ThermoFisher Element 2 single collector mass spectrometer. The repetition rate was set to 10 Hz using an energy density of ca. 5 J/cm^2 and spot size of 35 μm. The system was tuned on the NIST 612 reference material to yield a stable signal and high sensitivity for ^{139}La and ^{232}Th while keeping oxide production $<0.1\%$ ($^{232}Th^{16}O/^{232}Th$). The NIST 612 reference material was used as external and bracketing standard. Overall measurement time for a single analysis was 60 s, including 20 s for background measurement. Concentrations of the measured elements were calculated using GLITTER software (Griffin et al. 2008) using SiO_2 as internal standard element. Zircon reference material Z91500 was used as a monitor for precision and accuracy ($n = 8$), and reproducibility was better than 10% (2 RSD) for key trace elements (see online supplementary material).

3. Field relationships

In the southwest of the BGB, the Charlie gabbros and Moi–Moi metagabbros occur as km-sized bodies that are completely enclosed by the Kabalebo charnockites. Due to the location in dense tropical rainforest, the degree of exposure is very low and outcrops are generally small, isolated patches of rock in riverbeds and near small waterfalls. Hence, field relationships are difficult to discern and contacts between the gabbroic bodies and surrounding charnockite are very rarely exposed. An ambiguous contact can be seen at the Moi–Moi waterfall where thin granitic dykelets protrude from a charnockite vein into the metagabbro, suggesting that the metagabbro predates the charnockites (Fig. 2(c)). Such contacts, however, can be deceiving as the thin dykes could be the result of local re-melting of the charnockite upon intrusion of the gabbro (e.g. Claeson, 1999). The common occurrence of co-magmatic metadolerite enclaves in the charnockites (Fig. 2(b)) is indicative of magma mixing and mingling and suggests that charnockitic and mafic melts were emplaced contemporaneously (Klaver et al., 2015). These metadolerite enclaves represent quenched mafic melt globules that have an ophitic texture with minor secondary amphibole that are geochemically similar to the larger Moi–Moi metagabbro bodies. On this basis, we assert that the metadolerite enclaves are disaggregated fragments of the larger metagabbroic bodies that have mingled with the charnockitic melt, analogous to, e.g. Humphreys et al. (2009); Braschi et al. (2012).

4. Results

4.1 Sample description and U/Pb geochronology

4.1.1 Charlie gabbro ER 1115B. – Gabbro sample ER 1115B was taken from the centre of a well-exposed, km-sized body enclosed by Kabalebo charnockites in the southwest of the BGB (Fig. 1), roughly 1 km downstream from Charlie Falls. The contacts with the Kabalebo charnockite are not exposed. Sample ER 1115B is a coarse-grained leucogabbro with cumulate texture in which sub- to euhedral plagioclase is surrounded by intercumulus orthopyroxene (Figs. 2 and 3). Exsolved clinopyroxene lamellae are a common feature, which suggests the former presence of pigeonite. The characteristic olivine with corona texture is lacking in this sample. Scanning electron microscope (SEM) investigations showed that somewhat rounded baddeleyite is present as <20 μm grains in highly evolved melt pockets hosted predominantly in plagioclase. These melt pockets are crystallized to multiphase assemblages including clinopyroxene, apatite, late-stage ilmenite, Fe-oxides and baddeleyite (Fig. 3). Apart from the presence of secondary zircon as a thin rim around ilmenite, baddeleyite and magnetite in one of the melt pockets, no secondary alteration of baddeleyite to zircon or zirconolite is observed. Separation of sufficient grains proved to be challenging due to the very low concentration and small size of baddeleyite in sample ER 1115B. The two extracted baddeleyite fractions yield a mean $^{207}Pb/^{206}Pb$ age of 1971 ± 15 Ma (Fig. 4, Table 1). This age is

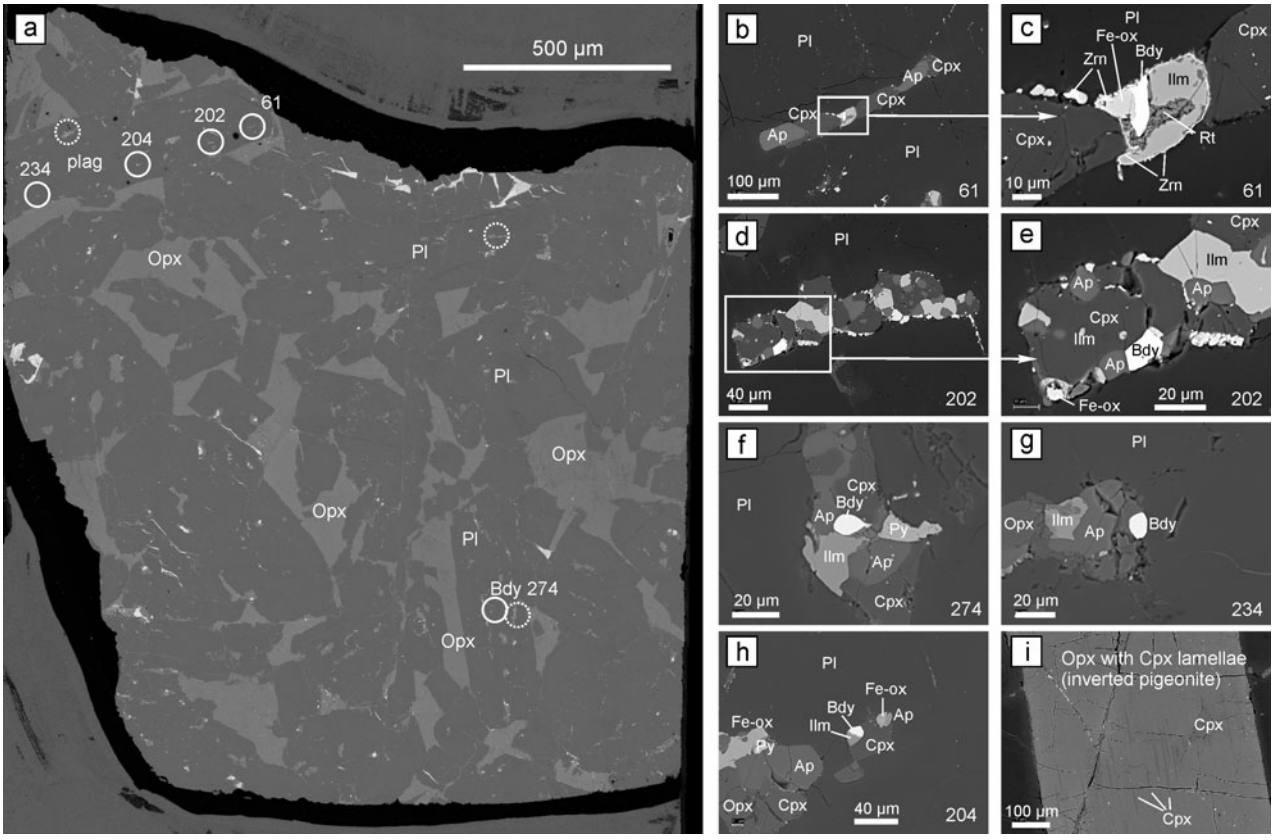

Fig. 3. BSE images showing the petrography of Charlie gabbro sample ER 1115B. The gabbro is essentially undeformed except for minor low-temperature cataclastic zones and fractures and has a coarse cumulate texture of euhedral plagioclase surrounded by ortho- and clinopyroxene. The exsolution textures in pyroxene indicate slow cooling from high temperatures. Circled areas indicate multiphase late-stage melt pockets that are shown in detail on the right. Baddeleyite (Bdy) is bright white in these BSE images. A rare zircon rim is seen in one spot (c). Mineral abbreviations are after Whitney & Evans (2010).

mostly controlled by the precise analysis of fraction 2, whereas fraction 1 has a large propagated error related to blank correction.

4.1.2 Moi–Moi metagabbro ER 1109. – Metagabbro sample ER 1109 is a fully recrystallized metagabbro of intermediate grain size that was sampled roughly 200 m upstream from the Moi–Moi waterfall from a well-exposed, km-sized mafic body surrounded by charnockite in the SW of the BGB (Fig. 1). The metagabbro has a granoblastic texture and contains an equilibrium mineral assemblage of clinopyroxene, orthopyroxene, plagioclase and blue-green amphibole (Fig. 5). Another sample from the same body, taken ~50 m away, shows variable overprint on the hand sample scale: recrystallized domains have a granoblastic texture similar to ER 1109, but there are also zones with less overprint that retain a relict ophitic texture as indicated by plagioclase laths surrounded by cm-sized brown-green intercumulus hornblende. The blue-green amphibole is a secondary phase that formed at the expense of clino- and orthopyroxene. Imaging by SEM revealed the presence of large zircon crystals (up to 500 µm in length) with complicated zoning patterns and embayments. No baddeleyite was encountered. The zircons are randomly distributed and do not reside in late-stage melt pockets, in contrast with baddeleyite in Charlie gabbro sample ER 1115B. BSE and CL imaging of the zircons reveals a complex internal zoning (Fig. 6). Based on the images, five textural zones can be distinguished. The larger grains show irregular, strongly embayed core domains (zone 1) that are characterized by a bright CL response. Central holes in the large zircons are probably parts of these CL bright domains

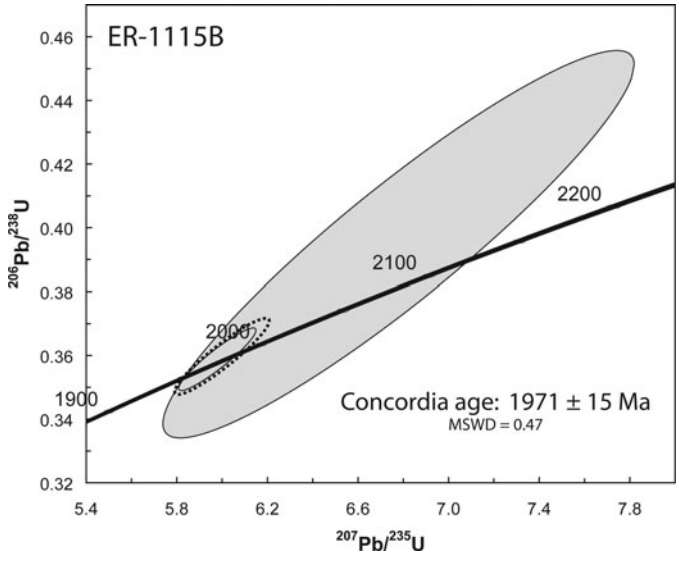

Fig. 4. Concordia diagram for the two baddeleyite fractions from Charlie gabbro sample ER 1115B. The two fractions yield a concordia age of 1971 ± 15 Ma (dashed ellipse).

Table 1. Baddeleyite U/Pb TIMS data for Charlie gabbro sample ER 1115B. (1) Pbc = common Pb, Pbtot = total Pb (radiogenic + blank + intitial); (2) measured ratio, corrected for fractionation and spike; (3) isotope ratio corrected for fractionation, spike contribution, blank and initial common Pb (see text for further discussion); (4) correlation coefficient between $^{206}Pb/^{238}U$ and $^{207}Pb/^{235}U$ ratios.

Sample	Th/U	Pbc/ Pbtot(1)	$^{206}Pb/^{204}Pb$(2)	$^{207}Pb^*/^{235}U$	1 s.e. %	$^{206}Pb^*/^{238}U$	1 s.e. %	rho(4)	$^{206}Pb/^{238}U$	1 s.e.	$^{207}Pb/^{235}U$	1 s.e.	$^{207}Pb/^{206}Pb$	1 s.e.
				ratios(3)					ages (Ma)					
ER 1115B														
Bd-a (6 grains)	0.33	1.047	35.8	6.7782	6.28	0.3950	6.26	0.93	2146	114	2083	56	2021	43
Bd-b (4 grains)	0.07	0.274	205.4	5.9756	1.17	0.3591	1.12	0.93	1978	19	1972	10	1967	8

95% confidence weighted mean $^{207}Pb/^{206}Pb$ date: 1971 ± 15 Ma

Table 2. Zircon U/Pb SIMS data for Moi–Moi metagabbro sample ER 1109. (1) radiogenic ^{206}Pb in percentage; (2) ratios corrected for common Pb using the measured ^{204}Pb; (3) correlation coefficient between $^{206}Pb/^{238}U$ and $^{207}Pb/^{235}U$ ratios; (4) U concentration calculated from measured $U/^{94}ZrO_2$ of zircon standard Z91500 with a concentration of 80 ppm U.

Sample	CL domain	$r^{206}Pb\%$(1)	$^{207}Pb^*/^{235}U$	1 s.e. %	$^{206}Pb^*/^{238}U$	1 s.e. %	rho(3)	$^{206}Pb/^{238}U$	1 s.e.	$^{207}Pb/^{235}U$	1 s.e.	$^{207}Pb/^{206}Pb$	1 s.e.	UO/U	Th/U	U(4) ppm
			ratios(2)					ages (Ma)								
ER 1109																
543z sp3	bright-1	97.7	6.998	8.2	0.3904	8.0	0.987	2125	145	2111	73	2098	23	7.72	0.57	73
585z sp3	bright-1	99.9	6.411	7.3	0.3605	7.1	0.983	1984	121	2034	64	2084	24	8.15	0.48	54
513z sp2	lt gr-4	99.9	5.624	7.7	0.3331	7.7	0.998	1854	124	1920	66	1992	8	7.83	0.73	140
513z sp1	med gr-2	100.0	5.580	7.4	0.3319	7.4	0.999	1848	119	1913	64	1985	3	7.95	1.17	467
585z sp2	med gr-2	99.9	5.795	8.0	0.3447	7.9	0.997	1909	131	1946	69	1984	10	7.74	0.68	110
585z sp4	dark-3	100.0	5.494	7.0	0.3270	7.0	0.999	1824	111	1900	60	1984	6	8.14	0.10	442
543z sp1	dark-3	100.0	5.844	7.9	0.3479	7.9	0.999	1925	132	1953	69	1983	4	7.74	1.71	539
543z sp4	dark-3	99.9	5.728	7.9	0.3419	7.9	0.999	1896	129	1936	68	1978	6	7.77	0.40	233
543z sp2	dark-3	99.9	5.732	8.1	0.3433	8.0	0.996	1902	132	1936	70	1972	13	7.72	0.71	84
585z sp5	rim gr-5	99.7	5.006	7.0	0.3034	7.0	0.998	1708	105	1820	59	1952	8	8.14	0.20	248
585z sp1	med gr-2	99.8	5.497	7.9	0.3344	7.9	0.997	1859	128	1900	68	1945	11	7.76	0.67	96

95% confidence weighted mean $^{207}Pb/^{206}Pb$ dates: 2091 ± 32 Ma, 1984 ± 4 Ma, 1950 ± 13 Ma

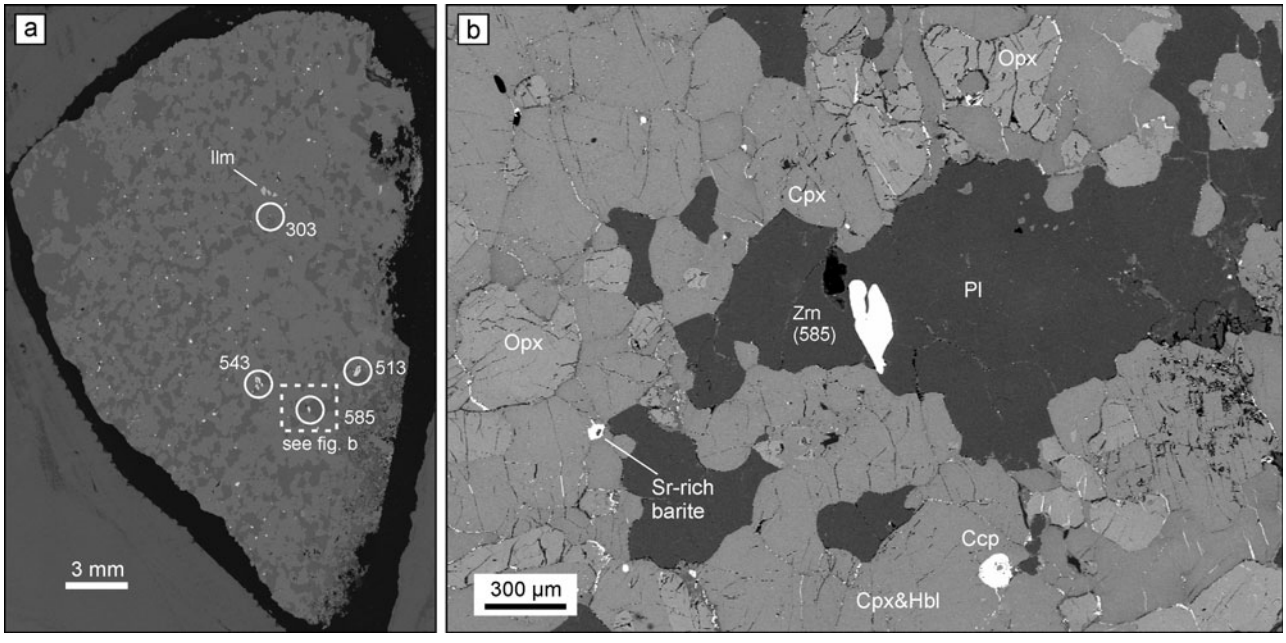

Fig. 5. BSE images of Moi–Moi metagabbro sample ER 1109; (a) overview of sample ER 1109, a fully recrystallized metagabbro with a high-grade granoblastic texture dominated by two pyroxenes (BSE mid grey) and plagioclase (BSE dark grey). The sample lacks an obvious foliation. Bright phases are large, complexly zoned zircon crystals (outlined by white circles), ilmenites and minor sulphides; (b) detailed view of the area outlined in (a), showing the granoblastic texture and one of the large, embayed zircon grains dated in this study. Mineral abbreviations are after Whitney & Evans (2010).

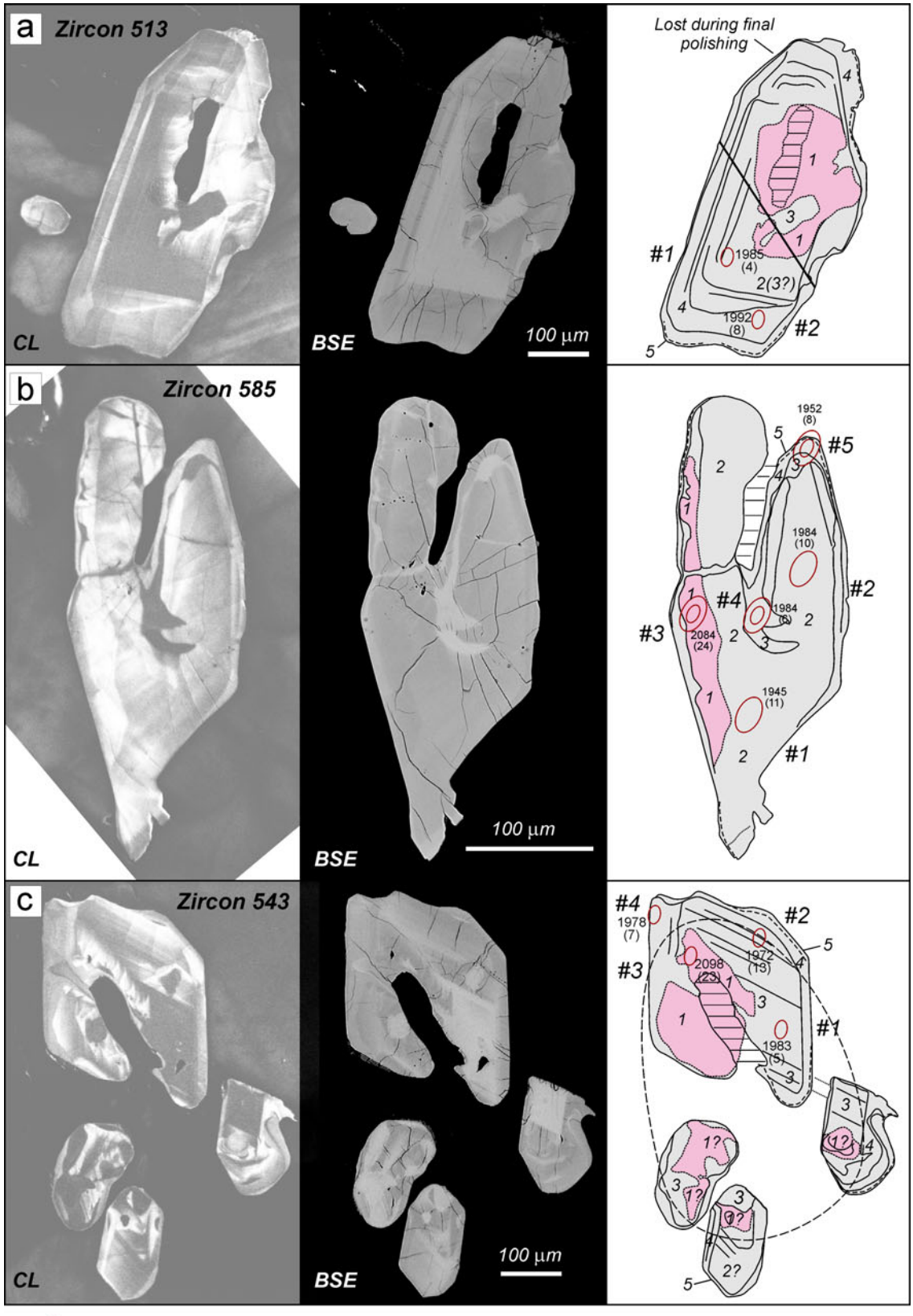
a
Zircon 513
CL
BSE
100 µm
Lost during final polishing
#1
1985 (4)
2(3?)
1992 (8)
#2
b
Zircon 585
CL
BSE
100 µm
1952 (8)
#5
1984 (10)
#2
#4
1984 (5)
#3
2084 (24)
1945 (11)
#1
c
Zircon 543
CL
BSE
100 µm
#4
1978 (7)
#2
1972 (13)
#3
2098 (23)
#1
1983 (5)
Older cores (1)
Central holes
Ion probe spot (~18x27 µm), located after analysis
Ion probe spot (<9x13 µm), with field aperture applied
#1 Ion probe spot, with age and uncertainty (1σ)

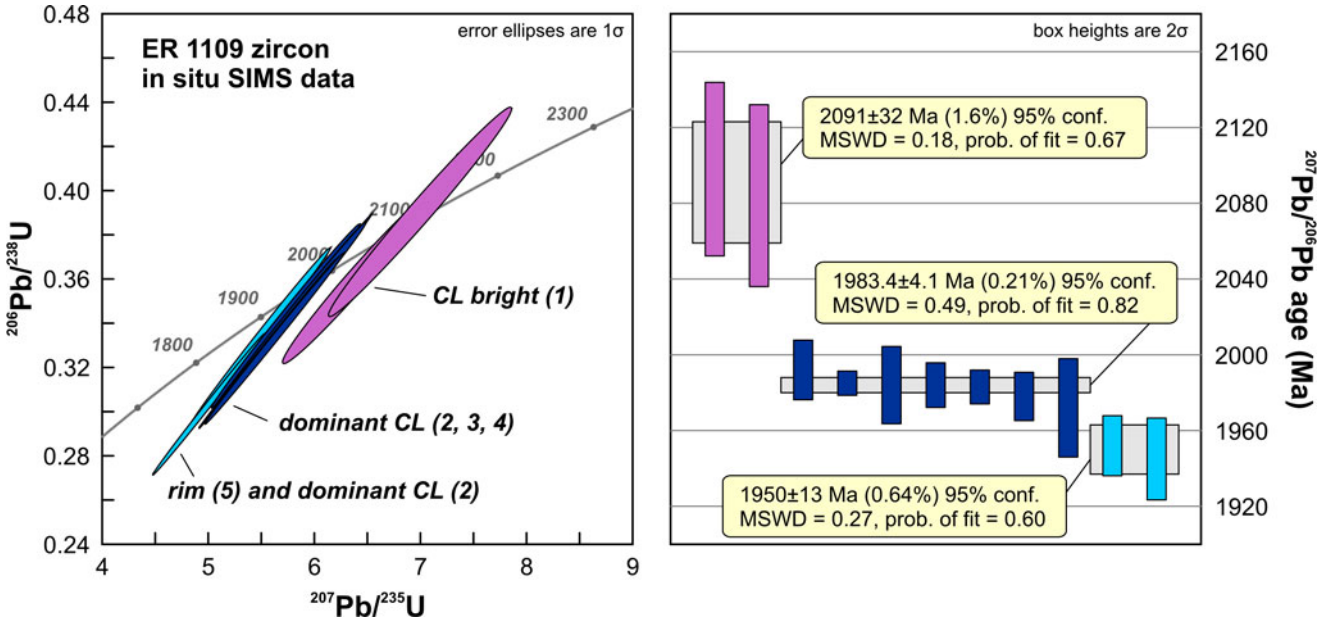

Fig. 7. U/Pb concordia diagram (left) and $^{207}Pb/^{206}Pb$ ages (right) with weighted means highlighted for the different age populations. The CL bright, irregular cores (violet) are inherited and match the age of UHT metamorphism in the area. The main growth domain (dark blue) yields an age of 1984 ± 4 Ma, which is identical to the 1984–1993 Ma age for the surrounding charnockites (Klaver et al., 2015). Two spots are younger (light blue) and reflect the timing of metamorphic recrystallization at 1950 ± 13 Ma.

that were plucked out during polishing, or could be the result of resorption. The major part of the zircon grains, the main growth domain, is formed by zones 2, 3 and 4. Zone 3 is bright in BSE and dark in CL, suggesting a higher U content compared to zone 2. Weak oscillatory zoning is developed in zones 2 and 3, which are separated from zone 4 by a clear discontinuity. Zone 4 shows variable CL characteristics and occasional concentric zoning. Locally, a thin, outermost rim (zone 5) is developed.

A total of 11 ion-probe spot analyses were acquired on different zircon grains and zones. The results are shown in Table 2 and Figs. 6 and 7. Two spot analyses in the highly resorbed, CL bright inner cores (zone 1) yield a weighted mean $^{207}Pb/^{206}Pb$ age of 2091 ± 32 Ma. Seven analyses of the dominant growth domains (zones 2–4) yield a weighted mean $^{207}Pb/^{206}Pb$ age of 1984 ± 4 Ma. Given the overall uncertainties, no significant age difference can be seen between zones 2 and 4. One spot analysis from a thin, outermost rim (zone 5) and one internal spot from the main growth domain (zone 2) yield a younger $^{207}Pb/^{206}Pb$ age of 1950 ± 13 Ma. Spot #1 in zircon grain 585 (Fig. 6) is located within CL/BSE zone 2. It either sampled a thin rim of zone 5 above the depth of CL excitation, or a local zone of alteration (Pb-loss) facilitated by the abundant nearby cracks, Fig. 6.

4.2 Zircon trace elements

The trace element composition of ER 1109 zircon is shown in Fig. 8 and the full data-set is available in the online supplementary material. The zircons have rare-earth element (REE) patterns typical of magmatic zircon, with steeply increasing REE contents from La to Lu and large and positive Ce-anomalies (Hoskin & Schaltegger, 2003). On the basis of the trace element data, two groups can be distinguished in the zircon population. A main group that comprises ca. 80% of the grains and a second group with higher U, Th, Nb and REE concentrations. The latter group corresponds to particularly BSE bright areas within zones 2–4 of the measured zircons. The hafnium concentration of the zircons varies from 6500 to 10 000 ppm and is positively correlated with most trace elements for the zircons in the main group.

4.3 Zircon hafnium isotopes

Measured Hf isotope compositions were age corrected using a decay constant of 1.867×10^{-11} year^{-1} (Söderlund et al., 2004) and the $^{207}Pb/^{206}Pb$ age of the main growth phase. CHUR values from Bouvier et al. (2008) were adopted to calculate initial ϵHf ($\epsilon Hf_{1984\ Ma}$) values (Fig. 9). A total of 47 spots in the main growth domains (zones 2–4) were analysed for hafnium isotope composition. Only two spot analyses were acquired in the CL bright, irregular cores (zone 1), while the outermost rims (zone 5) proved to be too thin for analysis. Initial ϵ_{Hf} at 1984 Ma for the main growth domain is highly uniform and ranges from −1.2 to +1.3 with a weighted average of 0.0 ± 0.2 (2 SD, $n = 47$). The two spots in CL bright, irregular zones are within

Fig. 6. CL, BSE and interpreted images of the complex zircons in Moi–Moi metagabbro sample ER 1109. Red ellipses indicate the exact locations of the ion probe pits. White lines trace additional zonation. Five distinct textural zones can be distinguished, in addition to the central holes that either represent empty inclusions, extreme resorption or older, metamict cores that were plucked out during polishing. Zone 1 represents CL bright, irregular cores. Zones 2, 3 and 4 comprise the main growth domain of the zircons. Zone 3 is typically BSE bright compared to zone 2, while zone 4 is a main rim overgrowth with concentric CL zoning. A thin, outermost rim is locally developed and constitutes zone 5. See text for further discussion.

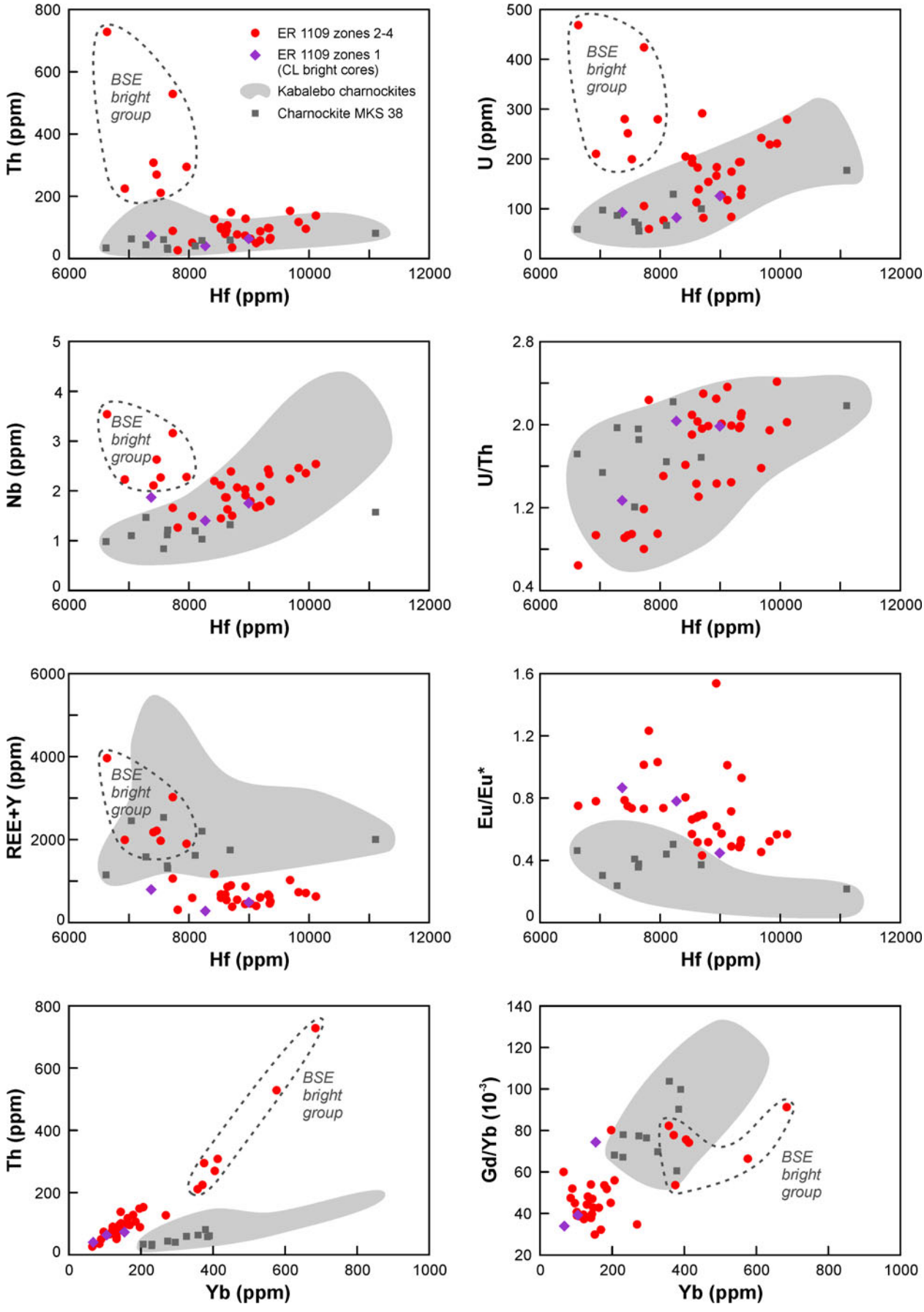
ER 1109 zones 2-4
ER 1109 zones 1 (CL bright cores)
Kabalebo charnockites
Charnockite MKS 38
BSE bright group
Th (ppm)
U (ppm)
Nb (ppm)
U/Th
REE+Y (ppm)
Eu/Eu*
Gd/Yb (10-3)
Hf (ppm)
Yb (ppm)

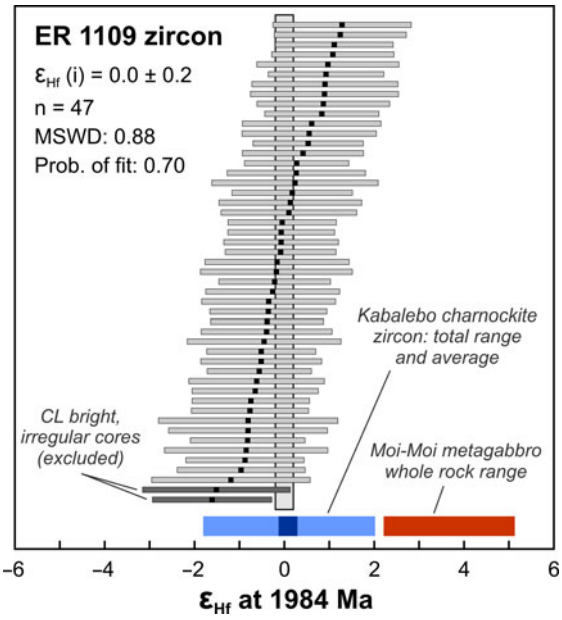

Fig. 9. Initial εHf at 1984 Ma of ER 1109 zircon. With the exception of two spots in CL bright, irregular, probably inherited cores at $\epsilon Hf_{1984\,Ma} = -1.5$, the zircons constitute a single, homogeneous population with an average $\epsilon Hf_{1984\,Ma}$ of 0. This value is identical to the average $\epsilon Hf_{1984\,Ma}$ of Kabalebo charnockite zircon (Klaver et al., 2015) but distinct from the whole rock $\epsilon Hf_{1984\,Ma}$ of the Moi–Moi metagabbros (Uunk, 2015).

error of this range at $\epsilon Hf_{1984\,Ma} = -1.5 \pm 1.6$ and -1.6 ± 1.3, although they are tendentially lower.

5. Discussion

5.1 *Timing of mafic magmatism in the BGB*

The new geochronological data, in conjunction with field observations, put new constraints on the timing of mafic magmatism in the BGB. The Charlie gabbros lack the metamorphic overprint that is characteristic for the Moi–Moi metagabbros. On this basis, we assert that the Charlie gabbros are younger than the Moi–Moi metagabbros. As baddeleyite U/Pb systematics are not readily reset during metamorphism or alteration, instead baddeleyite would rather react to form zircon or be lost completely (Heaman & LeCheminant, 1993), the 1971 ± 15 Ma baddeleyite $^{207}Pb/^{206}Pb$ age for sample ER 1115B can be confidently interpreted as the intrusion age of the Charlie gabbros. This age puts a lower limit on the age of intrusion and also the metamorphism of the Moi–Moi metagabbros.

The interpretation of the U/Pb results for the large zircons in sample ER 1109 is less straightforward, in particular due to the complex internal textures. The BSE and CL images combined with the U/Pb data provide evidence that the zircons contain inherited domains (zone 1), which formed at 2091 ± 32 Ma. This age is within error to the timing of the UHT metamorphic event in the BGB at 2073–2055 Ma (De Roever et al. 2003b; Klaver et al. 2015). Spot analyses in zones 2–4 yield an age of 1984 ± 4 Ma, which is identical to the 1984–1993 Ma age of zircon grains with typical magmatic zoning in the surrounding Kabalebo charnockites (Klaver et al. 2015). The complex internal resorption in the ER 1109 zircons makes it difficult to interpret the 1984 ± 4 Ma age and it could either date a metamorphic overprint leading to partial resetting of the U/Pb system, metamorphic zircon growth, zircon crystallization in the charnockite country rocks or zircon growth in the gabbroic melt. On the basis of the relict magmatic zoning and the occurrence of two discrete 2091 ± 32 Ma cores, metamorphic growth or resetting, respectively, appears implausible. Trace element and Hf isotope data also strongly argue against a metamorphic origin for the main growth domain, which is discussed in detail in Section 5.2. As metamorphic resetting or growth can be excluded, this implies that the main growth domain is magmatic in origin. Hence, the metagabbro zircons have crystallized either from the gabbroic melt or are magmatic grains derived from the country rocks through assimilation. The major internal resorption boundary that separates zones 2 and 3 from the main overgrowth (zone 4) and that gave the zircons their complex 3D geometry could be the result of the incorporation of the zircons in the gabbroic melt. In this scenario, zones 1 to 3 represent xenocrystic zircon that is inherited from the surrounding country rock, the Kabalebo charnockites, while zone 4 crystallized from the gabbroic melt and hence dates the timing of intrusion of the metagabbro. Alternatively, zones 2–4 could represent multiple phases of zircon growth and dissolution in the mafic melt. Complex internal resorption patterns for zircons that form a single age population, crystallizing from a variety of melt compositions, have been documented and do not always indicate a polyphase evolution (Hoskin & Schaltegger, 2003). The origin of the complex zircons is further discussed in Section 5.2, where trace element and Hf isotope data are presented. In both scenarios, however, the timing of metagabbro emplacement is tightly constrained. If zones 2–4 all crystallized from the gabbroic melt, the 1984 ± 4 Ma age dates gabbro emplacement. Else, if zones 2 and 3 are xenocrystic, the mean age for zones 2 and 3 provides a tight upper age limit, with a lower age limit of 1971 ± 15 Ma given by the age of the Charlie gabbros. As zones 2 and 3 and zone 4 yield analytically indistinguishable ages, the timing of the emplacement of the Moi–Moi metagabbro ER 1109 is tightly constrained at 1984 ± 4 Ma.

We interpret the late, outermost rims with an age of 1950 ± 13 Ma as a phase of subsolidus zircon growth, probably related to the thermal event that was responsible for the metamorphic overprint of the metagabbro. The 1950 ± 13 Ma age is within error of the 1971 ± 15 Ma baddeleyite age for the Charlie gabbros and therefore intrusion of the gabbros might be contemporaneous with this late thermal pulse. A thin, CL dark rim that resembles zone 5 in ER 1109 is seen around zircon in Kabalebo charnockite sample MKS 26 and to lesser extent MKS

Fig. 8. Trace element variation of ER 1109 zircon compared to the range displayed by the Kabalebo charnockites (Klaver et al., 2015). Zircon from charnockite sample MKS 38 is highlighted as this sample was taken close to the contact with the metagabbro and sampling location of ER 1109 at Moi–Moi waterfall. The ER 1109 zircons can be divided into two distinct trace element groups: a main group and a BSE bright group with higher Th, U, Nb and REE content. Eu/Eu* is calculated as $Eu_N/\sqrt{(Sm_N \times Gd_N)}$ where the subscript "N" denotes chondrite normalized values.

38 (Klaver et al., 2015). The latter charnockite sample is derived from the Moi–Moi waterfall, near the contact with the metagabbro and sampling locality of ER 1109. This suggests that part of the Kabalebo charnockites should have been affected by the thermal pulse as well, even though they do not show clear signs of metamorphic recrystallization.

5.2 *Origin of the complex zircons in ER 1109*

In the case that the large, complex zircons in the Moi–Moi metagabbro are xenocrystic, the 1984 ± 4 Ma age reflects the main growth phase of zircon in the country rock. This age is identical to the range in zircon U/Pb ages reported for the surrounding Kabalebo charnockites: 1984 ± 4 Ma to 1993 ± 5 Ma (Klaver et al., 2015). Hence, it is plausible that emplacement of the Moi–Moi metagabbros postdates the charnockites and that the zircon grains have been acquired through assimilation of the charnockite wall rock. Alternatively, the presence of co-magmatic metadolerite enclaves in the charnockites suggests that the metagabbros and Kabalebo charnockites might be contemporaneous and that the zircons in the metagabbro could be entrained during magma mingling. Klaver et al. (2015) have demonstrated that the Kabalebo charnockites are the product of melting of the UHT granulite suite. The presence of inherited cores with an age that matches the UHT event is thus not surprising. Such inherited cores, however, have not been identified in the charnockite zircon population, which is characterized by an absence of xenocrystic zircon. This is likely a result of sampling bias, as selection of charnockite zircons for U/Pb analysis was aimed towards euhedral zircon in the $<180\,\mu m$ size fraction, thereby neglecting larger grains that potentially include inherited domains.

To investigate whether the complex zircons in metagabbro ER 1109 are derived from the surrounding Kabalebo charnockites, the zircons have been analysed for their trace element and Hf isotope composition. Many attempts have been made to use trace element systematics of igneous zircon to identify its paragenesis (e.g. Heaman et al. 1990; Hoskin & Ireland 2000; Belousova et al. 2002; Grimes et al. 2007). In principle, zircon REE concentrations and slopes, U/Th and other geochemical characteristics should reflect the melt from which they crystallized. Due to the poorly constrained partition coefficients for zircon (Hanchar & van Westrenen 2007), however, it has proven to be challenging to resolve the subtle differences between zircon growing from felsic and mafic melts, and only zircon with mantle affinity can be satisfactorily resolved (Belousova et al. 2002). In the case of the metagabbro zircons, the availability of trace element and Hf data for zircon from the Kabalebo charnockites (Klaver et al. 2015) allows direct comparison.

Zircon from metagabbro ER 1109 can be divided into two distinct groups based on their trace element signature, including a fairly homogeneous main group and a second group of spots in BSE bright zones that is characterized by higher U, Th, Nb and REE contents but similar U/Th and Gd/Yb (Fig. 8). The CL bright inherited cores (zone 1) cannot be distinguished from the main growth domain (zones 2–4) on the basis of trace element characteristics. The main group of ER 1109 zircon displays a range in U/Th, Hf and Nb concentrations that overlaps with the Kabalebo charnockite zircon data. REE abundances and slopes, however, are different. Total REE concentrations are lower, Eu anomalies are smaller and heavy REE slopes (HREE, e.g. Gd/Yb) are lower in ER 1109 zircon than in zircon in the charnockites. The REE characteristics of the Moi–Moi zircons suggest equilibrium with a melt with lower HREE contents and a lower HREE slope (i.e. a flatter HREE pattern), which could indicate that the ER 1109 zircons crystallized from the gabbroic melt. On the basis of the ER 1109 zircon Hf data, however, this hypothesis must be rejected. Initial ϵHf at 1984 Ma of the main growth domain (zones 2–4) is highly uniform at an $\epsilon Hf_{1984\,Ma}$ of zero (Fig. 9), which is identical to the range in $\epsilon Hf_{1984\,Ma}$ displayed by the Kabalebo charnockite zircons (Klaver et al., 2015) but different from the whole rock $\epsilon Hf_{1984\,Ma}$ of this sample at around +4 (Uunk, 2015). An important implication of the difference between zircon and whole rock $\epsilon Hf_{1984\,Ma}$ is that the zircons were not in equilibrium with the metagabbroic melt and must be inherited from a different source, most likely the Kabalebo charnockites. This raises the question why REE characteristics are markedly different between the ER 1109 and charnockite zircon populations. In addition, the BSE and CL textures of the ER 1109 zircons are characterized by complex zoning and resorption while the charnockite zircons are typically euhedral with simple magmatic oscillatory and sector zoning. The identical Hf isotope composition but distinct textures and trace element characteristics can be explained by the entrainment of charnockite zircon in the gabbroic melt, leading to (i) resorption due to the incorporation in a melt that is undersaturated with respect to zircon and (ii) complex internal reorganization of trace elements by a coupled dissolution–reprecipitation process. It has been shown that the latter process can change zircon textures and trace element concentrations while leaving the Hf isotope composition unaffected (Gerdes & Zeh 2009; Lenting et al. 2010; Zeh et al. 2010). Due to its compatibility in the zircon crystal structure, Hf is not readily mobilized and will retain its original isotope composition even at granulite facies metamorphism. In contrast, the preferential purging of trace elements that are less compatible in the zircon crystal structure (e.g. the REEs) compared to more compatible elements such as Hf, Th and U is a possible mechanism to explain the relative depletion in REE in ER 1109 zircon (Hoskin & Schaltegger 2003; Geisler et al. 2007). This would also explain the steeper HREE slopes as LREEs are less compatible than HREEs in zircon. In the case of the ER 1109 zircons, the relict oscillatory zoning attests to an originally magmatic origin, but incorporation of the zircons in the gabbroic melt caused partial resetting of the trace element characteristics.

The obvious conclusion resulting from the good agreement in $\epsilon Hf_{1984\,Ma}$ is that the complex zircons in metagabbro ER 1109 are derived from the Kabalebo charnockites. It is tempting to regard these zircons as xenocrysts and relate their presence in the metagabbro to assimilation of the charnockite country rock, which implies that the Moi–Moi metagabbros postdate charnockite emplacement. We propose a different explanation, namely crystal transfer during mingling of the gabbroic and charnockitic melts, on the basis of the following observations: (i) the U/Pb dates for zone 4, which overgrows the major resorption boundary associated with the incorporation of the zircons in the gabbroic melt, are statistically indistinguishable from zones 2 and 3 and (ii) comagmatic metadolerite enclaves are common in the charnockites, and these can petrographically and geochemically be related to the metagabbroic bodies. In our proposed scenario, mingling of the gabbroic and charnockitic

melts is responsible for the occurrence of the metadolerite enclaves, which represent disaggregated fragments of the larger metagabbro bodies. Even if extensive mixing and hybridization between two melts are not always obvious, the mechanical transfer of phenocrysts from enclaves to the host rock and vice versa is well documented (e.g. Barbarin & Didier 1992; Elburg 1996a; Humphreys et al. 2009; Foley et al. 2013; Braschi et al. 2014). We propose that this process of crystal transfer is responsible for the occurrence of charnockitic zircon in the metagabbro. Klaver et al. (2015) argued that zircon was an early crystallizing phase in the Kabalebo charnockites, which enabled the mechanical transfer of zircon into the gabbroic bodies. If zircon would have been a late crystallizing phase, the high degree of solidification in the charnockitic mush must have significantly hindered mingling of the two melts and crystal transfer. In the proposed scenario of crystal transfer, the zircons in metagabbro ER 1109 are neither autocrysts (i.e. grown from the melt in which they are situated), nor are they antecrysts or xenocrysts *sensu stricto* (Miller et al., 2007). The term "antecryst", a grain that crystallized from an earlier pulse of magma, comes closest to covering the origin of these grains and hence we refer to them as "transferred antecrysts". The occurrence of similar transferred zircon antecrysts in comagmatic mafic bodies has been demonstrated for other granitoid intrusions, where the mafic bodies often display a bimodal distribution in zircon initial ϵHf with an autocrystic zircon population originating from the mafic melt and transferred antecrysts from the felsic host (Elburg 1996b; Kemp et al. 2007; Yang et al. 2007; Li et al. 2009). The absence of an autocrystic zircon population in ER 1109 suggests that the metagabbroic melt remained undersaturated in silica and was not capable of crystallizing zircon. Baddeleyite might have formed in late stage melt pockets, but was subsequently lost during the thermal event that caused the metamorphic overprint.

5.3 *Implications for the evolution of the BGB*

The main conclusion of the U/Pb dating of the late Transamazonian mafic bodies in the BGB is that the Moi–Moi metagabbros are coeval with the Kabalebo charnockites (1984 Ma) and that the Charlie gabbros (1971 Ma) represent a slightly younger mafic pulse. Hence, the new geochronological data provide firm support for the model of Klaver et al. (2015), in which the voluminous Moi–Moi gabbroic magmatism was associated with and the heat source for the second UHT event in the BGB. The Kabalebo charnockites are spatially and temporally associated with a ca. 1400 km long belt of felsic metavolcanic rocks and subvolcanic granites that extends from Venezuela to Suriname, the CSID-belt (Fig. 1), even though they appear to be derived from distinct sources (Klaver et al. 2015). The CSID-belt felsic rocks show highly uniform ages of 1.99–1.98 Ga (Reis et al. 2000; Delor et al. 2003a; Nadeau et al. 2013; De Roever et al. in press) and hence are coeval with the emplacement of the Moi–Moi metagabbros. In the light of the regional distribution of the Moi–Moi metagabbros in the south-central Guiana Shield and their temporal association with the CSID-belt and Kabalebo charnockites, the Moi–Moi metagabbros appear to represent a phase of mantle perturbation and enhanced heat input into the Guiana Shield crust that was a direct cause of the late Transamazonian granitoid magmatism. The origin of the Moi–Moi metagabbros, however, is far from established. In several aspects, they are not like typical plume-related LIPs (Ernst 2014). The combination of gabbroic and ultramafic rocks within a single body, round to oval shape of the bodies, rough vertical and in cases concentric zoning and ubiquity of intercumulus hornblende (Bosma et al. 1983) strongly resembles subduction-related Alaskan-type mafic-ultramafic complexes. Alaskan-type complexes typically occur at convergent plate boundaries, have a distinct internal structure and composition and are generally interpreted as the root zones of arc complexes (e.g. Irvine 1974; Spandler et al. 2003; Batanova et al. 2005; Dhuime et al. 2009; Jagoutz & Schmidt 2013). One distinguishing feature of the Moi–Moi bodies is the common occurrence of magmatic orthopyroxene, which is generally rare in Alaskan-type complexes. There are, however, other examples of Precambrian mafic-ultramafic complexes akin to the Alaskan-type that do contain significant orthopyroxene (e.g. Brügmann et al. 1997; Helmy et al. 2014). Hence, a subduction-related origin for the Moi–Moi metagabbros, in combination with the new geochronological data, provides the first direct evidence for the inferred development of a convergent margin and northward subduction underneath the North Guiana TTG-greenstone belt during the late phase of the Transamazonian Orogeny (2.01–1.95 Ga; Fraga et al. 2009; Klaver et al. 2015). Further geochemical studies are, however, required to confirm the subduction zone geodynamic setting and petrogenesis of the Moi–Moi metagabbros. The recognition of the Moi–Moi metagabbros as subduction-related Alaskan-type complexes has an important implication for the use of the 1984 ± 4 Ma age of ER 1109 as precise bar for the barcode reconstruction of the Guiana Shield. In contrast to LIPs that are typically short lived, arc magmatism can continue for tens of Myr. Hence, the emplacement of the Moi–Moi metagabbros throughout the south-central Guiana Shield might have occurred intermittently over similar timescales.

6. Conclusions

Two generations of late Transamazonian mafic intrusive bodies have been recognized in the Bakhuis Granulite Belt. The first generation comprises hornblende-bearing, mafic to ultramafic complexes that occur widespread to the south of the north Guiana TTG-greenstone belt in Brazil, Guyana and Suriname. Where they are intruded in the Cauarane-Coeroeni Belt and BGB, these Moi–Moi bodies are characterized by a variable degree of granoblastic recrystallization and the growth of secondary, blue-green amphibole. The Moi–Moi metagabbro bodies are interpreted as Alaskan-type mafic-ultramafic complexes associated with the root zones of arc magmatism on the southern margin of the TTG-greenstone belt. Large zircons with complex zoning patterns and embayments are found in a sample of the Moi–Moi metagabbros from the BGB. CL and BSE imaging of the zircons revealed five distinct textural zones, which yield three distinct age populations. Highly irregular, CL bright cores represent an inherited domain with an age of 2091 ± 32 Ma, which corresponds to the ultrahigh-temperature metamorphic event in the BGB. The main growth domain of the complex zircons yields an age of 1984 ± 4 Ma and thin outermost rims are dated at 1950 ± 13 Ma. The presence of inherited cores and a perfect match of the 1984 ± 4 Ma age of the main growth domain with the zircon U/Pb ages reported for

the Kabalebo charnockites suggests that the complex zircons are derived from the surrounding charnockites. This hypothesis is confirmed by trace element and Hf isotope characteristics of the metagabbro zircons. Although the REEs show signs of partial re-equilibration with the gabbroic melt, U/Th, U, Th, Nb and Hf overlap with data for the Kabalebo charnockites. In addition, an initial ϵHf of zero for the complex zircons is identical to charnockite zircon but clearly distinct from the whole rock $\epsilon Hf_{1984\ Ma}$ at +4. On the basis of the occurrence of metadolerite enclaves in the charnockites, we conclude that the gabbroic and charnockitic melts are contemporaneous and interacted through mingling. Hence, the complex zircons in the metagabbro are not xenocrysts *sensu stricto*, but are interpreted as "transferred antecrysts" that originated from the charnockitic melt and were mechanically transferred to the metagabbroic enclaves and bodies. The presence of primary brown hornblende and a metamorphic overprint distinguishes the Moi–Moi metagabbros from a younger suite of gabbros. The non-metamorphic, amphibole-free Charlie gabbros postdate the Moi–Moi metagabbros. The 1971 ± 15 Ma baddeleyite U/Pb age is within error of the 1950 ± 13 Ma age of the outermost rims in the metagabbro zircon, suggesting that gabbro emplacement could be synchronous with the thermal event that caused the metamorphic overprint. The 1.98–1.97 Ga ages for the two generations of gabbroic intrusions in the BGB confirm that mafic magmatism was contemporaneous with and the likely heat source for charnockite emplacement. The late Transamazonian age of the gabbroic intrusions clearly postdates the UHT metamorphic event in the BGB at 2.07–2.05 Ga, and leaves the origin of the UHT event enigmatic.

Acknowledgements – MK, EdR and AT are very thankful to the staff of Kabalebo Nature Resort and in particular Karel and Joyce Dawson for facilitating fieldwork in the Bakhuis Mountains. The Dr Schürmann Foundation provided financial support for the field campaigns and analytical work (grants 53/2008 and 87/2012), and the Stichting Molengraaff Fund covered additional fieldwork costs of MK and AT. This manuscript benefited from thoughtful comments made by three anonymous reviewers and careful editorial handling by Martin Klausen. This is publication no. 41 of the Large Igneous Provinces – Supercontinent Reconstruction – Resource Exploration Project (www.supercontinent.org; NSERC CRDPJ 419503-11: CAMIRO Project 08E03.

Disclosure statement

No potential conflict of interest was reported by the authors.

Supplementary materials

Supplemental material for this article is available via the supplemental tab on the article's online page at http://dx.doi.org/10.1080/11035897.2015.1061591.

References

Barbarin, B. & Didier, J., 1992: Genesis and evolution of mafic microgranular enclaves through various types of interaction between coexisting felsic and mafic magmas. *Transactions of the Royal Society of Edinburgh: Earth Sciences 83* (*1–2*), 145–153. doi:10.1017/S0263593300007835.

Batanova, V., Pertsev, A., Kamenetsky, V., Ariskin, A., Mochalov, A. & Sobolev, A., 2005: Crustal evolution of island-arc ultramafic magma: Galmoenan pyroxenite–dunite plutonic complex, Koryak highland (Far East Russia). *Journal of Petrology 46* (*7*), 1345–1366. doi:10.1093/petrology/egi018.

Belousova, E., Griffin, W.L., O'Reilly, S.Y. & Fisher, N., 2002: Igneous zircon: trace element composition as an indicator of source rock type. *Contributions to Mineralogy and Petrology 143* (*5*), 602–622. doi:10.1007/s00410-002-0364-7.

Berrangé, J.P., 1977: *The geology of southern Guyana, South America*, HM Stationery Office, London. 112 pp.

Bosma, W., Kroonenberg, S., Maas, K. & De Roever, E., 1983: Igneous and metamorphic complexes of the Guiana Shield in Suriname. *Geologie en Mijnbouw 62*, 241–254.

Bouvier, A., Vervoort, J.D. & Patchett, P.J., 2008: The Lu-Hf and Sm-Nd isotopic composition of CHUR: Constraints from unequilibrated chondrites and implications for the bulk composition of terrestrial planets. *Earth and Planetary Science Letters 273* (*1-2*), 48–57. doi:10.1016/j.epsl.2008.06.010.

Braschi, E., Francalanci, L., Tommasini, S. & Vougioukalakis, G.E., 2014: Unraveling the hidden origin and migration of plagioclase phenocrysts by in situ Sr isotopes: the case of final dome activity at Nisyros volcano, Greece. *Contributions to Mineralogy and Petrology 167* (*3*), 1–25. doi:10.1007/s00410-014-0988-4.

Braschi, E., Francalanci, L. & Vougioukalakis, G.E., 2012: Inverse differentiation pathway by multiple mafic magma refilling in the last magmatic activity of Nisyros Volcano, Greece. *Bulletin of Volcanology 74* (*5*), 1083–1100. doi:10.1007/s00445-012-0585-1.

Brügmann, G., Reischmann, T., Naldrett, A. & Sutcliffe, R., 1997: Roots of an Archean volcanic arc complex: the Lac des Iles area in Ontario, Canada. *Precambrian Research 81*, 223–239.

Claeson, D.T., 1999: Geochronology of the Rymmen gabbro, southern Sweden; implications for primary versus inherited zircon in mafic rocks and rheomorphic dykes. *GFF 121* (*1*), 25–31. doi:10.1080/11035899901211025.

Clark, C., Fitzsimons, I.C., Healy, D. & Harley, S.L., 2011: How does the continental crust get really hot? *Elements 7* (*4*), 235–240. doi:10.2113/gselements.7.4.235.

Collins, W., 2002: Hot orogens, tectonic switching, and creation of continental crust. *Geology 30* (*6*), 535–538. doi:10.1130/0091-7613(2002)030<0535:HOTSAC>2.0.CO;2.

Compston, W., Williams, I. & Meyer, C., 1984: U-Pb geochronology of zircons from lunar breccia 73217 using a sensitive high mass-resolution ion microprobe. *Journal of Geophysical Research: Solid Earth (1978–2012) 89*, B525–B534.

Corfu, F., Hanchar, J.M., Hoskin, P.W. & Kinny, P., 2003: Atlas of zircon textures. *Reviews in Mineralogy and Geochemistry 53* (*1*), 469–500. doi:10.2113/0530469.

da Rosa-Costa, L., Lafon, J., Cocherie, A. & Delor, C., 2008: Electron microprobe U–Th–Pb monazite dating of the transamazonian metamorphic overprint on Archean rocks from the amapá block, southeastern Guiana Shield, Northern Brazil. *Journal of South American Earth Sciences 26* (*4*), 445–462. doi:10.1016/j.jsames.2008.05.007.

da Rosa-Costa, L.T., Lafon, J.M. & Delor, C., 2006: Zircon geochronology and Sm-Nd isotopic study: Further constraints for the Archean and Paleoproterozoic geodynamical evolution of the southeastern Guiana Shield, north of Amazonian Craton, Brazil. *Gondwana Research 10* (*3–4*), 277–300. doi:10.1016/j.gr.2006.02.012.

De Roever, E.W.F., Kroonenberg, S.B., Delor, C. & Phillips, D., 2003a: The Käyser dolerite, a Mesoproterozoic alkaline dyke suite from Suriname. *Geologie de la France 2–3–4*, 161–174.

De Roever, E.W.F., Lafon, J.-M., Delor, C., Cocherie, A., Guerrot, C. & De Artigo, A., in press: Orosirian magmatism and metamorphism in Surinam: new geochronological constraints. In *Contribuições à Geologia da Amazônia*. Sociedade Brasileira de Geologia - Núcleo Norte, Belém.

De Roever, E.W.F., Lafon, J.-M., Delor, C., Cocherie, A., Rossi, P., Guerrrot, C. & Potrel, A., 2003b: The Bakhuis ultrahigh-temperature granulite belt (Suriname): I. petrological and geochronological evidence for a counter-clockwise P–T path at 2.07–2.05 Ga. *Geologie de la France 2–3–4*, 175–205.

Delor, C., De Roever, E.W.F., Lafon, J.-M., Lahondère, D., Rossi, P., Cocherie, A., Guerrrot, C. & Potrel, A., 2003a: The Bakhuis ultrahigh-temperature granulite belt (Suriname): II. implications for late Transamazonian crustal stretching in a revised Guiana Shield framework. *Geologie de la France 2–3–4*, 207–230.

Delor, C., Lahondère, D., Egal, E., Lafon, J.-M., Cocherie, A., Guerrot, C., Rossi, P., Truffert, C., Théveniaut, H., Phillips, D. & De Avelar, V.G., 2003b: Transamazonian crustal growth and reworking as revealed by the 1:500,000-scale geological map of French Guiana (2nd edition). *Geologie de la France 2–34*, 5–57.

Dhuime, B., Bosch, D., Garrido, C.J., Bodinier, J.-L., Bruguier, O., Hussain, S.S. & Dawood, H., 2009: Geochemical Architecture of the Lower- to Middle-crustal Section of a Paleo-island Arc (Kohistan Complex, Jijal-Kamila Area, Northern Pakistan): Implications for the Evolution of an Oceanic Subduction Zone. *Journal of Petrology 50* (*3*), 531–569. doi:10.1093/petrology/egp010.

Elburg, M.A., 1996a: Evidence of isotopic equilibration between microgranitoid enclaves and host granodiorite, Warburton Granodiorite, Lachlan Fold Belt, Australia. *Lithos 38* (*1–2*), 1–22. doi:10.1016/0024-4937(96)00003-5.

Elburg, M.A., 1996b: U-Pb ages and morphologies of zircon in microgranitoid enclaves and peraluminous host granite: evidence for magma mingling. *Contributions to Mineralogy and Petrology 123* (*2*), 177–189. doi:10.1007/s004100050149.

Ernst, R.E., 2014: *Large igneous provinces*, Cambridge University Press, Cambridge. 666 pp.

Foley, F.V., Pearson, N.J., Rushmer, T., Turner, S. & Adam, J., 2013: Magmatic evolution and magma mixing of Quaternary adakites at Solander and Little Solander Islands, New Zealand. *Journal of Petrology 54* (*4*), 703–744. doi:10.1093/petrology/egs082.

Fraga, L.M., Reis, N.J. & Dall'Agnol, R., 2009: Cauarane-Coeroeni Belt-The main tectonic feature of the Central Guyana Shield. *Northern Amazonian Craton. Simpósio de Geologia da Amazônia 11*, 2–5.

Geisler, T., Schaltegger, U. & Tomaschek, F., 2007: Re-equilibration of zircon in aqueous fluids and melts. *Elements 3* (*1*), 43–50. doi:10.2113/gselements.3.1.43.

Gerdes, A. & Zeh, A., 2006: Combined U-Pb and Hf isotope LA-(MC-) ICP-MS analyses of detrital zircons: comparison with SHRIMP and new constraints for the provenance and age of an Armorican metasediment in Central Germany. *Earth and Planetary Science Letters 249* (*1-2*), 47–61. doi:10.1016/j.epsl.2006.06.039.

Gerdes, A. & Zeh, A., 2009: Zircon formation versus zircon alteration—new insights from combined U–Pb and Lu–Hf in-situ LA-ICP-MS analyses, and consequences for the interpretation of Archean zircon from the Central Zone of the Limpopo Belt. *Chemical Geology 261* (*3-4*), 230–243. doi:10.1016/j.chemgeo.2008.03.005.

Gibbs, A.K. & Barron, C.N., 1993: *The geology of the Guiana Shield*, 258 Oxford University Press, Oxford.

Griffin, W., Powell, W., Pearson, N., O'Reilly, S. & GLITTER: 2008: data reduction software for laser ablation ICP-MS. *Laser Ablation-ICP-MS in the Earth Sciences. Mineralogical Association of Canada Short Course Series 40*, 204–207.

Grimes, C., John, B., Kelemen, P., Mazdab, F., Wooden, J., Cheadle, M., Hanghøj, K. & Schwartz, J., 2007: Trace element chemistry of zircons from oceanic crust: a method for distinguishing detrital zircon provenance. *Geology 35* (*7*), 643–646. doi:10.1130/G23603A.1.

Grove, M., Jacobson, C.E., Barth, A.P. & Vucic, A., 2003: Temporal and spatial trends of Late Cretaceous-early Tertiary underplating of Pelona and related schist beneath southern California and southwestern Arizona. In S.E. Johnson, S.R. Paterson, J.M. Fletcher, G.H. Girty, D.L. Kimbrough & A. Martin-Barajas (eds.): *Tectonic Evolution of Northwestern Mexico and the Southwestern USA*, 381–406. Geological Society of America, special paper 374.

Guo, J., Peng, P., Chen, Y., Jiao, S. & Windley, B.F., 2012: UHT sapphirine granulite metamorphism at 1.93–1.92 Ga caused by gabbronorite intrusions: implications for tectonic evolution of the northern margin of the North China Craton. *Precambrian Research 222-223*, 124–142. doi:10.1016/j.precamres.2011.07.020.

Hanchar, J.M. & van Westrenen, W., 2007: Rare Earth Element Behavior in Zircon-Melt Systems. *Elements 3* (*1*), 37–42. doi:10.2113/gselements.3.1.37.

Heaman, L. & LeCheminant, A., 1993: Paragenesis and U–Pb systematics of baddeleyite (ZrO_2). *Chemical Geology 110* (*1-3*), 95–126. doi:10.1016/0009-2541(93)90249-I.

Heaman, L.M., Bowins, R. & Crocket, J., 1990: The chemical composition of igneous zircon suites: implications for geochemical tracer studies. *Geochimica et Cosmochimica Acta 54* (*6*), 1597–1607. doi:10.1016/0016-7037(90)90394-Z.

Helmy, H.M., Abd El-Rahman, Y.M., Yoshikawa, M., Shibata, T., Arai, S., Tamura, A. & Kagami, H., 2014: Petrology and Sm-Nd dating of the Genina Gharbia Alaskan-type complex (Egypt): Insights into deep levels of Neoproterozoic island arcs. *Lithos 198-199*, 263–280. doi:10.1016/j.lithos.2014.03.028.

Hildebrand, R.S., Buchwaldt, R. & Bowring, S.A., 2014: On the allochthonous nature of auriferous greenstones, Guayana shield, Venezuela. *Gondwana Research 26* (*3-4*), 1129–1140. doi:10.1016/j.gr.2013.09.011.

Hoskin, P.W. & Ireland, T.R., 2000: Rare earth element chemistry of zircon and its use as a provenance indicator. *Geology 28* (*7*), 627–630. doi:10.1130/0091-7613(2000)28<627:REECOZ>2.0.CO;2.

Hoskin, P.W.O. & Schaltegger, U., 2003: The composition of zircon and igneous and metamorphic petrogenesis. *Reviews in Mineralogy and Geochemistry 53* (*1*), 27–62. doi:10.2113/0530027.

Humphreys, M.C., Christopher, T. & Hards, V., 2009: Microlite transfer by disaggregation of mafic inclusions following magma mixing at Soufrière Hills volcano, Montserrat. *Contributions to Mineralogy and Petrology 157* (*5*), 609–624. doi:10.1007/s00410-008-0356-3.

Irvine, T.N., 1974: Petrology of the Duke Island ultramafic complex southeastern Alaska. *Geological Society of America Memoirs 138*, 1–244.

Jagoutz, O. & Schmidt, M., 2013: The composition of the foundered complement to the continental crust and a re-evaluation of fluxes in arcs. *Earth and Planetary Science Letters 371–372*, 177–190. doi:10.1016/j.epsl.2013.03.051.

Kemp, A.I.S., Hawkesworth, C.J., Foster, G.L., Paterson, B.A., Woodhead, J.D., Hergt, J.M., Gray, C.M. & Whitehouse, M.J., 2007: Magmatic and Crustal Differentiation History of Granitic Rocks from Hf-O Isotopes in Zircon. *Science 315* (*5814*), 980–983. doi:10.1126/science.1136154.

Klaver, M., de Roever, E.W., Nanne, J.A., Mason, P.R. & Davies, G.R., 2015: Charnockites and UHT metamorphism in the Bakhuis Granulite Belt, western Suriname: Evidence for two separate UHT events. *Precambrian Research 262*, 1–19. doi:10.1016/j.precamres.2015.02.014.

Kroonenberg, S.B. & de Roever, E.W., 2010: Geological evolution of the Amazonian Craton. *In* C. Hoorn & F.P. Wesselingh (eds.): *Amazonia: Landscape and Species Evolution: A look into the past*, 7–28.

Lenting, C., Geisler, T., Gerdes, A., Kooijman, E., Scherer, E.E. & Zeh, A., 2010: The behavior of the Hf isotope system in radiation-damaged zircon during experimental hydrothermal alteration. *American Mineralogist 95* (*8–9*), 1343–1348. doi:10.2138/am.2010.3521.

Li, X., Li, W., Wang, X., Li, Q., Liu, Y. & Tang, G., 2009: Role of mantle-derived magma in genesis of early Yanshanian granites in the Nanling Range, South China: in situ zircon Hf-O isotopic constraints. *Science in China Series D: Earth Sciences 52* (*9*), 1262–1278. doi:10.1007/s11430-009-0117-9.

Liu, X., Jahn, B.-m., Zhao, Y., Li, M., Li, H. & Liu, X., 2006: Late Pan-African granitoids from the Grove Mountains, East Antarctica: age, origin and tectonic implications. *Precambrian Research 145* (*1–2*), 131–154. doi:10.1016/j.precamres.2005.11.017.

Ludwig, K.R., 2012: *Isoplot/Ex Version 4: A Geochronological Toolkit For Microsoft Excel*. Berkeley Geochronology Center. 75 pp. Berkeley.

Miller, J.S., Matzel, J.E., Miller, C.F., Burgess, S.D. & Miller, R.B., 2007: Zircon growth and recycling during the assembly of large, composite arc plutons. *Journal of Volcanology and Geothermal Research 167* (*1–4*), 282–299. doi:10.1016/j.jvolgeores.2007.04.019.

Minter, W.E.L., 2006: The sedimentary setting of Witwatersrand placer mineral deposits in an Archean atmosphere. *Geological Society of America Memoirs 198*, 105–119.

Morel, M.L.A., Nebel, O., Nebel-Jacobsen, Y.J., Miller, J.S. & Vroon, P.Z., 2008: Hafnium isotope characterization of the GJ-1 zircon reference material by solution and laser-ablation MC-ICPMS. *Chemical Geology 255* (*1-2*), 231–235. doi:10.1016/j.chemgeo.2008.06.040.

Nadeau, S., Chen, W., Reece, J., Lachhman, D., Ault, R., Faraco, M.T.L., Fraga, L.M., Reis, N.J. & Betiollo, L.M., 2013: Guyana: the Lost Hadean crust of South America? *Brazilian Journal of Geology 43* (*4*), 601–606. doi:10.5327/Z2317-48892013000400002.

Norcross, C., Davis, D.W., Spooner, E.T. & Rust, A., 2000: U–Pb and Pb–Pb age constraints on Paleoproterozoic magmatism, deformation and gold mineralization in the Omai area, Guyana Shield. *Precambrian Research 102* (*1–2*), 69–86. doi:10.1016/S0301-9268(99)00102-3.

Paces, J.B. & Miller, J.D., 1993: Precise U–Pb ages of Duluth Complex and related mafic intrusions, northeastern Minnesota: Geochronological insights to physical, petrogenetic, paleomagnetic, and tectonomagmatic processes associated with the 1.1 Ga Midcontinent Rift System. *Journal of Geophysical Research: Solid Earth (1978–2012) 98*, 13997–14013.

Padoan, M., Rossetti, P. & Rubatto, D., 2014: The choco 10 gold deposit (El Callao, Bolivar State, Venezuela): petrography, geochemistry and U–Pb geochronology. *Precambrian Research 252*, 22–38. doi:10.1016/j.precamres.2014.06.024.

Peng, P., Guo, J., Windley, B., Liu, F., Chu, Z. & Zhai, M., 2012: Petrogenesis of late paleoproterozoic liangcheng charnockites and s-type granites in the central-northern margin of the North China Craton: implications for ridge subduction. *Precambrian Research 222–223*, 107–123. doi:10.1016/j.precamres.2011.06.002.

Reis, N.J., De Faria, M.S.G., Fraga, L.M. & Haddad, R.C., 2000: Orosirian calc-alkaline volcanism and the Orocaima event in the northern Amazonian Craton, eastern Roraima state, Brazil. *Revista Brasileira de Geociencias 30*, 380–383.

Reis, N.J., Teixeira, W., Hamilton, M.A., Bispo-Santos, F., Almeida, M.E. & D'Agrella-Filho, M.S., 2013: Avanavero mafic magmatism, a late Paleoproterozoic LIP in the Guiana Shield, Amazonian Craton: U-Pb ID-TIMS baddeleyite, geochemical and paleomagnetic evidence. *Lithos 174*, 175–195. doi:10.1016/j.lithos.2012.10.014.

Santos, J.O.S., Potter, P.E., Reis, N.J., Hartmann, L.A., Fletcher, I.R. & McNaughton, N.J., 2003: Age, source, and regional stratigraphy of the Roraima Supergroup and Roraima-like outliers in northern South America based on U-Pb geochronology. *Geological Society of America Bulletin 115*, 331–348. doi:10.1130/0016-7606(2003)115<0331:ASARSO>2.0.CO;2.

Santos, J.O.S., Van Breemen, O.B., Groves, D.I., Hartmann, L.A., Almeida, M. E., McNaughton, N.J. & Fletcher, I.R., 2004: Timing and evolution of multiple Paleoproterozoic magmatic arcs in the Tapajós Domain, Amazon Craton: constraints from SHRIMP and TIMS zircon, baddeleyite and titanite U–Pb geochronology. *Precambrian Research 131* (*1-2*), 73–109. doi:10.1016/j.precamres.2004.01.002.

Santosh, M., Liu, S., Tsunogae, T. & Li, J., 2012: Paleoproterozoic ultrahigh-temperature granulites in the North China Craton: implications for tectonic models on extreme crustal metamorphism. *Precambrian Research 222–223*, 77–106. doi:10.1016/j.precamres.2011.05.003.

Schmitt, A.K., Chamberlain, K.R., Swapp, S.M. & Harrison, T.M., 2010: In situ U-Pb dating of micro-baddeleyite by secondary ion mass spectrometry. *Chemical Geology 269* (*3–4*), 386–395. doi:10.1016/j.chemgeo.2009.10.013.

Schmitz, M.D., Bowring, S.A. & Ireland, T.R., 2003: Evaluation of Duluth Complex anorthositic series (AS3) zircon as a U–Pb geochronological standard: New high-precision isotope dilution thermal ionization mass spectrometry results. *Geochimica et Cosmochimica Acta 67* (*19*), 3665–3672. doi:10.1016/S0016-7037(03)00200-X.

Söderlund, U. & Johansson, L., 2002: A simple way to extract baddeleyite (ZrO2). *Geochemistry, Geophysics, Geosystems 3*, 1–7.

Söderlund, U., Patchett, P.J., Vervoort, J.D. & Isachsen, C.E., 2004: The 176Lu decay constant determined by Lu–Hf and U–Pb isotope systematics of Precambrian mafic intrusions. *Earth and Planetary Science Letters 219*, 311–324.

Spandler, C.J., Arculus, R.J., Eggins, S.M., Mavrogenes, J.A., Price, R.C. & Reay, A.J., 2003: Petrogenesis of the Greenhills Complex, Southland, New Zealand: magmatic differentiation and cumulate formation at the roots of a Permian island-arc volcano. *Contributions to Mineralogy and Petrology 144* (*6*), 703–721. doi:10.1007/s00410-002-0424-z.

Stacey, J.S. & Kramers, J.D., 1975: Approximation of terrestrial lead isotope evolution by a two-stage model. *Earth and Planetary Science Letters 26* (*2*), 207–221. doi:10.1016/0012-821X(75)90088-6.

Steiger, R.H. & Jäger, E., 1977: Subcommission on geochronology: convention on the use of decay constants in geo-and cosmochronology. *Earth and Planetary Science Letters 36* (*3*), 359–362. doi:10.1016/0012-821X(77)90060-7.

Uunk, B., 2015: *Geochemistry of mafic magmatism in the Bakhuis Granulite Belt, western Suriname; implications for UHT metamorphism.* MSc thesis, VU University Amsterdam, Amsterdam.

Westphal, M., Schumacher, J.C. & Boschert, S., 2003: High-temperature metamorphism and the role of magmatic heat sources at the Rogaland anorthosite complex in Southwestern Norway. *Journal of Petrology 44* (*6*), 1145–1162. doi:10.1093/petrology/44.6.1145.

Whitney, D.L. & Evans, B.W., 2010: Abbreviations for names of rock-forming minerals. *American Mineralogist 95* (*1*), 185–187. doi:10.2138/am.2010.3371.

Yang, J.-H., Wu, F.-Y., Wilde, S.A., Xie, L.-W., Yang, Y.-H. & Liu, X.-M., 2007: Tracing magma mixing in granite genesis: in situ U–Pb dating and Hf-isotope analysis of zircons. *Contributions to Mineralogy and Petrology 153* (*2*), 173–190. doi:10.1007/s00410-006-0139-7.

Zeh, A., Gerdes, A., Barton, J. & Klemd, R., 2010: U-Th-Pb and Lu-Hf systematics of zircon from TTG's, leucosomes, meta-anorthosites and quartzites of the Limpopo Belt (South Africa): constraints for the formation, recycling and metamorphism of Palaeoarchaean crust. *Precambrian Research 179* (*1–4*), 50–68. doi:10.1016/j.precamres.2010.02.012.

Zhang, Z., Zhao, G., Santosh, M., Wang, J., Dong, X. & Shen, K., 2010: Late Cretaceous charnockite with adakitic affinities from the Gangdese batholith, southeastern Tibet: Evidence for Neo-Tethyan mid-ocean ridge subduction? *Gondwana Research 17* (*4*), 615–631. doi:10.1016/j.gr.2009.10.007.